GBT AND cFSM: TWO MODAL APPROACHES TO THE BUCKLING ANALYSIS OF UNBRANCHED THIN-WALLED MEMBERS

S. Ádány[1*], N. Silvestre[2], B.W. Schafer[3] and D. Camotim[2]

[1]*Department of Structural Mechanics, Budapest University of Technology and Economics, 1111 Budapest, Műegyetem rkp. 3, Hungary*
[2]*Department of Civil Engineering and Architecture, Technical University of Lisbon, ICIST/IST, Av. Rovisco Pais, 1049 Lisboa, Portugal*
[3]*Department of Civil Engineering, Johns Hopkins University, Latrobe Hall 210, Baltimore, MD 21218, USA*
**(Corresponding author: E-mail: sadany@epito.bme.hu)*

ABSTRACT: The objective of this paper is to provide (i) the fundamental derivation details and (ii) a comparison between Generalised Beam Theory (GBT) and the constrained Finite Strip Method (cFSM), two alternative modal approaches to analyse the elastic buckling behaviour of unbranched thin-walled members. Thin-walled members may generally buckle in three families (or types) of modes: global, distortional and local (or local-plate) modes. The distinguishing feature of the GBT and cFSM methodologies to obtain buckling solutions is that they can formally separate these three types of buckling modes. An overall comparison of the two methods is provided, including practical aspects, such as the different notations, and theoretical points related to how the displacement fields are either constructed or decomposed into deformation modes akin to the above families. Specific derivation details are provided for both GBT and cFSM, along with numerical examples concerning the buckling behaviour of cold-formed steel lipped channel members under compression and bending. The numerical examples (i) show the power of both GBT and cFSM to separate general stability solutions into pure solutions related to the buckling mode types, (ii) illustrate the use of the identified deformation fields to examine the modal contributions to a buckling solution, and (iii) demonstrate that, in spite of their quite distinct developments, GBT and cFSM modal approaches provide essentially the same extended capabilities for examining and understanding thin-walled member stability. Moreover, considerable attention is also paid to the different handling of the membrane deformations by the two methods, which is responsible for the minor (but fully explainable) discrepancies existing between the results yielded by the two methods.

Keywords: Thin-walled members, buckling analysis, generalised beam theory (GBT), constrained finite strip method (cFSM), deformation modes, local buckling, distortional buckling, global buckling

1. INTRODUCTION

Since the load-carrying capacity of thin-walled members is often governed by buckling phenomena, the ability to calculate the corresponding elastic critical loads/moments is of paramount importance. However, the member ultimate load is very seldom close to its elastic critical load, due to (i) the physical non-linearity (plasticity effects), (ii) the presence of material and geometrical imperfections and (iii) the possible existence of a more or less pronounced post-buckling strength reserve. While physical non-linearity is associated primarily with the material constitutive behaviour, the imperfection-sensitivity and post-buckling strength reserve are tied to the nature of the buckling phenomenon (mode). This explains why the correct identification and classification of the buckling modes, as well as the accurate calculation of the corresponding critical loads, have chief importance in determining the ultimate load-carrying capacity of a thin-walled member.

Usually, three main families of buckling phenomena (modes) are encountered in practice: (i) global buckling, in which the member axis deforms (*e.g.*, flexural or lateral-torsional buckling), (ii) local-plate buckling, involving only plate (wall) bending, and (iii) distortional buckling, combining wall bending with cross-section distortion – the last two phenomena are sometimes jointly described as "local buckling". Although there exist several numerical and/or analytical methods to determine critical load/moment values and the corresponding buckling mode shapes, it is fair to say that only generalised beam theory

(GBT – *e.g.*, [1-3]) and the constrained finite strip method (cFSM – [4-6]) are able to perform this task for selected isolated ("pure") or arbitrarily combined ("coupled") modes.

For more than a decade, GBT has been the only approach possessing the modal features described above, which are specially useful to solve many problems of practical interest and, in particular, to provide in-depth understanding about several mechanical aspects of the member buckling behaviour. However, a novel modal approach has been recently developed and reported, namely the constrained finite strip method. Although the two approaches lead to very similar solutions, GBT and cFSM have quite different roots: while GBT is an extension of the classical thin-walled beam theory, the cFSM has its origins in the folded-plate theory underlying the semi-analytical finite strip method. Indeed, it may be said that (i) GBT is the generalisation of the classical beam theory, by considering additional degrees of freedom to allow for the cross-section in-plane deformations, whilst (ii) cFSM is a specialisation of the classical folded-plate theory that carefully selects constraints to force the member to deform (buckle) according to pre-defined patterns.

For about a year and a half the authors have been working on providing an in-depth comparison of the fundamentals of the two above modal approaches (GBT and cFSM), namely by addressing (i) their basic mechanical assumptions, (ii) the distinct procedures they employ, (iii) their domains of application and limitations, and also (iv) the numerical results provided by each of them [7-9] – therefore, the objective of this paper is to report in detail the outcome of the first phase of this ongoing research project. Initially, a general comparison is presented in section 2, which includes several practical aspects, such as the different notations, and theoretical points related to how the displacement fields are either constructed or decomposed into deformation modes akin to the three buckling mode families. Then, sections 3 and 4 are devoted to the presentation of the GBT and cFSM procedures to obtain the cross-section deformation modes. However, due to space limitations, the presentations are necessarily brief and cannot cover all the details – they rather focus on the main steps of the derivations and on the most important formulae involved (the interested reader can find more detailed information in the references). Next, illustrative numerical results concerning the buckling behaviour of lipped channel columns and beams are compared in section 5: the analyses are performed by means of the two approaches and the calculated critical loads and moments, together with the corresponding buckling mode participation factors, are presented and discussed. In particular, considerable attention is paid to the different handling of the membrane deformations, which is responsible for the minor (but fully explainable) discrepancies existing between the results yielded by the two methods – particularly the ones associated with column flexural buckling. Finally, the paper closes with some conclusions drawn from the comparison of the two modal approaches to analyse the buckling behaviour of unbranched open thin-walled members.

The authors hope that the comparison presented here will contribute to provide a better understanding of the two methodologies and also of the phenomena that they aim to uncover, thus paving the way to the development of more efficient tools for the analysis and design of thin-walled members, namely cold-formed steel columns, beams and beam-columns.

2. GENERAL COMPARISON BETWEEN GBT AND CFSM

2.1 Notation and Terminology

Consider the thin-walled member shown in Figure 1, which displays an arbitrary unbranched open cross-section formed by several walls (plate elements). The most important notation and terminology adopted by GBT and cFSM buckling analysis are summarised and compared in Table 1 – since the differences are not negligible, the interested reader is advised to pay attention to them, so that he can

fully grasp the similarities and differences between the main concepts and procedures involved in the two approaches, as well understand the buckling results yielded by either of them.

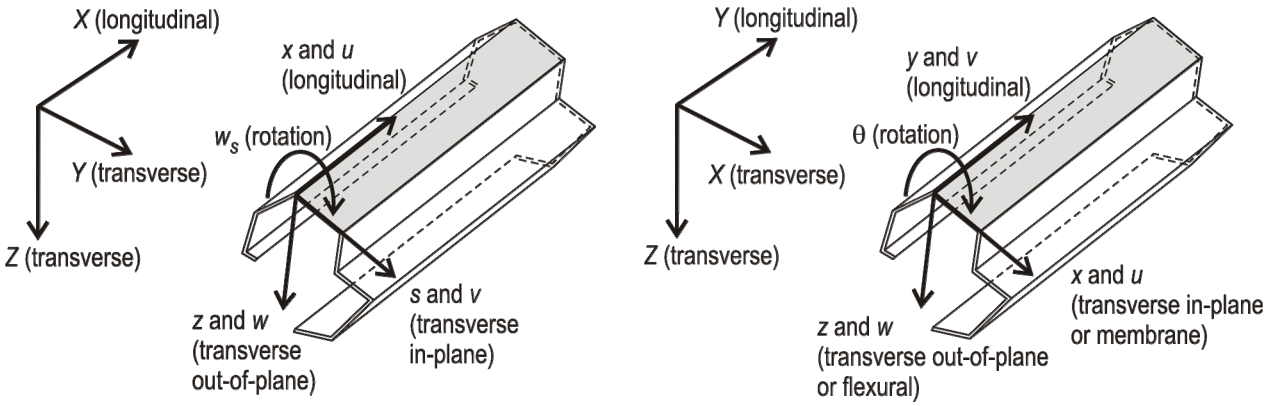

(a) GBT (b) cFSM

Figure 1. Thin-walled Member with Arbitrary Unbranched Open Cross-section: (a) GBT and (b) cFSM Coordinate Axis and Degree of Freedom Notations

Table 1. Comparisons between the Notation and Terminology Adopted by GBT and cFSM

	Description	**GBT**	**cFSM**
Displacements	longitudinal, transverse in-plane, transverse out-of-plane, rotation	$u, v, w, w_{,s}$	v, u, w, θ
Local coordinates	longitudinal, in-plane, out-of-plane	x, s, z	y, x, z
Global coordinates	longitudinal, transverse	X and Y, Z	Y and X, Z
Member	Length	L	a
	wall (plate) width	b	b
Nodes, DOF	node at wall ends	natural node	main node
	node within walls	intermediate node	sub-node
	number of walls	n	n_{main}-1
	intermediate/sub-node number	m	n_{sub}
	total number of DOF	$n+m+1$	$m = 4\times(n_{main}+n_{sub})$
Deformation modes	Global	rigid-body, global, G	global, G
	Distortional	distortional, D	distortional, D
	local plate	local-plate, LP	local, L
	Shear	shear, S	other, O
	transverse extension	shear, TE	other, O

2.2 Comparison at a Glance

Table 2 provides a schematic general overview of the essential features characterising the GBT and cFSM approaches, making it possible to draw some conclusions compare them and draw some conclusions about their similarities and differences. First of all, it is worth pointing out that, although they originate from different theories and exhibit quite distinct evolutions, the two methods handle the buckling analysis of thin-walled members in manners that exhibit many common traits. The most important similarity is the fact that both (i) begin by performing a *nodal* discretisation of the cross-section (*nodal* degrees of freedom) and (ii) end up reaching (defining) a set of cross-section deformation modes (*modal* degrees of

freedom). Conversely, the most important differences are related to (i) the longitudinal discretisation, (ii) the transformation to the modal basis and (iii) the concepts and procedures involved in the derivation and application of the two methods – some of these differences are discussed further ahead, in subsection 2.3.

Table 2. Comparison between the Essential Features of GBT and cFSM

Basis	**GBT**	**cFSM**
Origin	beam theory	folded-plate theory
Development of the method	enrichment of beam theory by adding additional deformation possibilities	decomposition of the general finite strip method deformation space
Two-step analysis	yes, first cross-section analysis, then member analysis	yes, first modal decomposition, then member analysis
Cross-section properties	calculation of modal cross-section properties, then the member treated as a bar	no cross-section properties are necessary, all the calculation is based on the strips
Orthogonal modes	important, not indispensable	possible, not crucial
Orthogonalisation	auxiliary eigenvalue problems in the cross-section (infinitesimal member element)	eigenvalue problem in member (longitudinal distribution is sin/cos)
Considered deformation modes	global, distortional, local-plate, shear, transverse extension	global, distortional, local, other
Base system for solution	always modal	can be modal or nodal
Cross-section discretisation	yes	yes
Distinction between main nodes and sub-nodes	yes	yes
DOF per node	u,v,w for natural nodes w for intermediate nodes	u,v,w,θ for all nodes – but any DOF can be switched off
Longitudinal discretisation	yes (if necessary)	never, due to FSM rational
Longitudinal displacement variation	no discretisation: sine-cosine discretisation: Hermite cubic polynomials	sine-cosine (in theory, it can be different – not yet worked out for cFSM)

As far as longitudinal discretisation is concerned, GBT allows for the application of the finite element method (beam elements adopting Hermite cubic polynomials for the longitudinal discretisation) or other numerical techniques, such as the finite difference, Rayleigh-Ritz or Galerkin methods – this possibility is particularly relevant if the member is not simply supported. However, for simply supported members (end sections locally/globally pinned and free to warp), trigonometric (sinusoidal) shape functions provide exact solutions for the problem and longitudinal discretisation can be avoided without sacrificing accuracy. In the case of cFSM, which retains the essence of finite strip analysis, longitudinal discretisation is never considered – recall that this is the key feature differentiating the FSM from the FEM (shell elements). Although the FSM has been implemented with various longitudinal shape functions, the cFSM uses only trigonometric (sinusoidal) longitudinal shape functions. Table 3 summarises how the different ways of handling the longitudinal shape functions affect the domains of application of the two methods.

Table 3. Comparison between the Domains of Application of GBT and cFSM

Applicability	**GBT**	**cFSM**
End restraint conditions	various: pinned, fixed, free, restrained/free warping	hinged and free to warp
Cross-section change along length	not allowed	not allowed
Tapered members	not	not
Intermediate supports along length	yes	yes, but only continuous

Another important difference between GBT and cFSM concerns the base systems adopted. cFSM begins by using mechanical assumptions to define sub-spaces for the various deformation mode families (G, D, L and O). Among the various cFSM base systems, it is possible to introduce a GBT-like one (see subsection 4.10), which can be determined by solving eigenvalue problems within the various sub-spaces – however, it should be emphasised that the calculation of pure buckling modes does not require any special base system in cFSM (the only important issue is the determination of the sub-spaces). Finally, note that, as far as the application of the cFSM is concerned, the adoption of the GBT-like base vectors does not entail any computational advantage.

In GBT, the determination of special (orthogonal) base vectors is fundamentally similar to the one employed by the cFSM and requires the solution of a sequence of auxiliary eigenvalue problems, defined for a cross-section (*i.e.*, a member element with an infinitesimal length dx) – in the cFSM, on the other hand, a "unit-length" member is analysed. Moreover, the existence of an orthogonal base system plays an important practical role in GBT, as the corresponding special base vectors are always associated with significant computational advantages (strong reduction of the number of degrees of freedom involved in the analyses).

2.3 Concepts and Procedures Adopted in the Derivations

Figure 2 provides flowcharts that briefly describe most of the concepts and (mostly) procedures involved in determining the deformation modes by means of GBT or the cFSM. Great emphasis is placed on the procedures adopted by these two methods to handle the various deformation mode families: (i) while GBT adds progressively more displacement degrees of freedom (d.o.f.) to the classical beam theory ones, (ii) the cFSM constrains the classical finite strip displacement degrees of freedom (d.o.f.). As it will be illustrated later, the numbers of displacement d.o.f. associated with the application of the two methods can be practically identical, even if they approach the thin-walled member analysis in fundamentally different ways. It is important to mention that figure 2 shows clearly that GBT gradually enhances of the deformation mode set, a sequential procedure that also reflects the historical evolution of the method – as for the cFSM, the sequential procedure displayed includes the steps that had to necessarily be followed to derive the method.

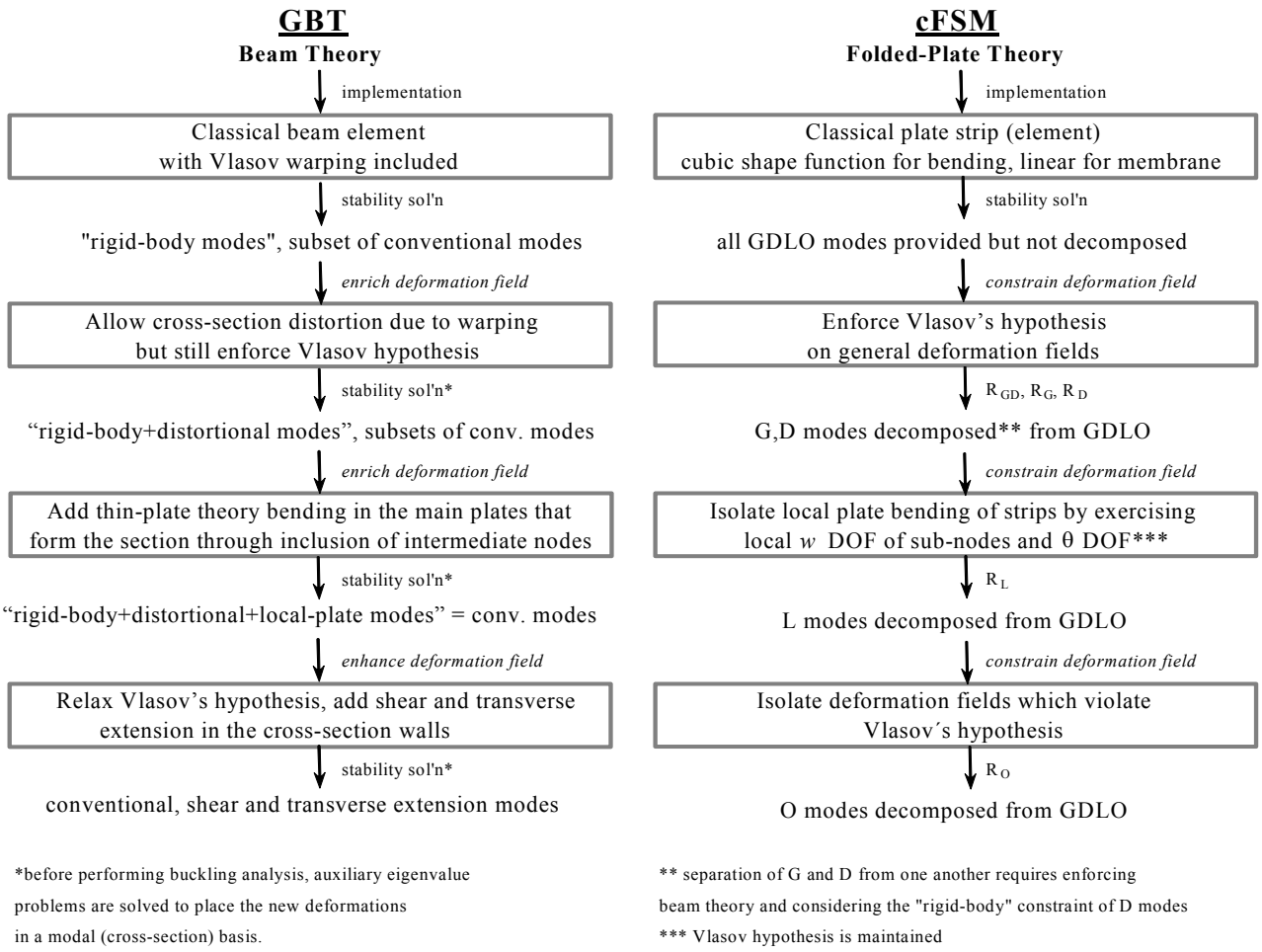

Figure 2. Flowcharts Concerning the Determination of the Deformation Mode by Means of GBT and cFSM

3. OVERVIEW OF GBT

First of all, it must be said that most of the unique features associated to the application of GBT stem from its cross-section analysis procedure, which has been described in detail in [1, 10] and leads to the identification of several (orthogonal) cross-section *deformation modes*: axial extension, major/minor axis bending, torsion, distortional and local-plate (transverse bending) modes. In order to provide a quick and concise overview of the most important concepts and procedures involved in the performance of a cross-section analysis, its application to the lipped channel section depicted in Figure 3 is briefly described and commented.

3.1 Cross-Section Analysis

A cross-section comprising n walls must be discretised into (i) $n+1$ natural nodes (wall ends) and (ii) m intermediate nodes, where it should be noted that the cross-section (free) end nodes are treated as *both* natural and intermediate, *i.e.*, are associated with a warping function *and* a local flexural function, thus making it possible to account for the flexural deformation of the end walls. (While the natural nodes are indispensable to perform a GBT analysis, the incorporation of intermediate nodes is necessary whenever the flexural deformation of the cross-section walls is relevant (mostly in local-plate buckling)). Figure 3 shows a possible discretisation of a lipped channel section that involves *6* natural nodes (mandatory) and *7* intermediate nodes (optional).

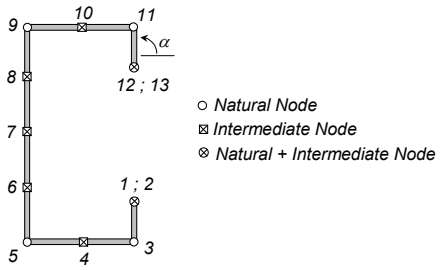

Figure 3. GBT Discretisation of a Lipped Channel Cross-Section.

In order to obtain the cross-section displacement field components (*i.e.*, functions $u(s)$, $v(s)$ and $w(s)$), one must begin by imposing (i) unit warping displacements at the natural nodes ($\overline{u}_k$ *=1, k=1, ..., n+1*) and (ii) unit flexural displacements at the intermediate nodes ($\overline{w}_k$ *=1, k=n+2, ..., n+m+1*), a procedure leading to the identification of *n+1* "elementary warping functions" $\overline{u}_k(s)$ and *m* "elementary local flexural functions" $\overline{w}_k(s)$, all varying linearly between consecutive nodes – Figure 4 displays the functions $\overline{u}_k(s)$ and $\overline{w}_k(s)$ associated with the lipped channel discretisation shown in Figure 3.

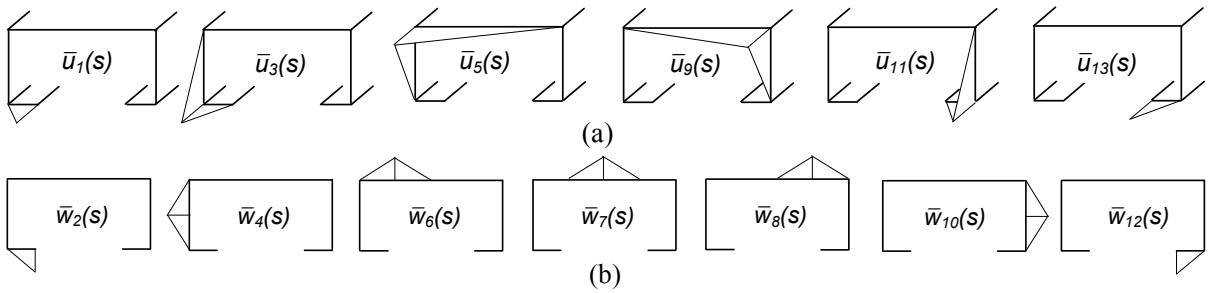

Figure 4. Lipped Channel Section Elementary (a) Warping ($\overline{u}_k(s)$) and (b) Local Flexural ($\overline{w}_k(s)$) Functions

In order to comply with Vlasov's assumption of null membrane shear strains along the cross-section mid-line, when a unit warping displacement is imposed at node *k* (function $u_k(s)$) each wall adjacent to that node is forced to move laterally, thus exhibiting membrane displacements *v* given by

$$\gamma_{xs} = u_{,s} + v_{,x} = 0 \qquad \Rightarrow \qquad \mathrm{dv} = -\frac{du}{ds}dx \tag{1}$$

Note that the elementary flexural functions $w_k(s)$ automatically satisfy Vlasov's assumption (since $u=v=0$). To ensure nodal compatibility between the transverse membrane (v) and flexural (w) displacements, the cross-section is "forced" to deform in its own plane due to the application of the "elementary warping functions" $\overline{u}_k(s)$. This is illustrated in Figure 5, where one sketches the membrane (v) and flexural (w) displacements associated with the $\overline{u}_k(s)$ and $\overline{w}_k(s)$ corresponding to a half (symmetric) lipped channel section.

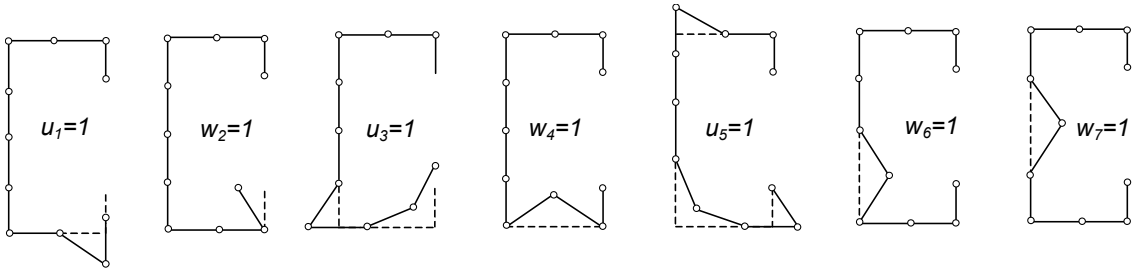

Figure 5. Deformed Configuration of the Cross-Section Walls after Imposing Unit Warping and Flexural Functions.

Imposing the wall membrane (v) and flexural (w) displacements leads to relative rotations between adjacent walls that violate the node compatibility, thus requiring the determination of nodal transverse bending moments that ensure rotation compatibility at the various nodes – this involves the solution of a statically indeterminate folded-plate problem, a task performed by means of the force method. (This could also be done by means of the displacement method. In the case of unbranched open cross-sections, both methods involve approximately the same amount of calculations.) When both equilibrium and compatibility are satisfied, one obtains the cross-section displacement field, characterised by (i) linear $u_k(s)$, constant $v_k(s)$ and cubic $w_k(s)$, in the case of $\overline{u}_k(s)$, and by (ii) null $u_k(s)$, null $v_k(s)$ and cubic $w_k(s)$, in the case of $\overline{w}_k(s)$. Then, the GBT equilibrium equation system is written in a vector space defined by a mixed coordinate system ($u_r(s)$ and $w_l(s)$): $y_k(s)$, with $k=1, ..., n+m+1$). For the discretisation shown in Figure 3, the mixed vector $\mathbf{y}$ of dimension $n+m+1$ reads

$$\mathbf{y} = \{u_1 \;\; w_2 \;\; u_3 \;\; w_4 \;\; u_5 \;\; w_6 \;\; w_7 \;\; w_8 \;\; u_9 \;\; w_{10} \;\; u_{11} \;\; w_{12} \;\; u_{13}\}^{\mathsf{T}} \tag{2}$$

The displacement fields obtained through the imposition of the various elementary functions are grouped in matrices $\mathbf{U}$, $\mathbf{V}$ and $\mathbf{W}$ (dimension $p \times (n+m+1)$, where p is the number of cross-section wall segments). The cross-section displacement field may then be expressed as

$$\mathbf{u} = \mathbf{U}\boldsymbol{\phi}_{,x} \qquad \mathbf{v} = \mathbf{V}\boldsymbol{\phi} \qquad \mathbf{w} = \mathbf{W}\boldsymbol{\phi} \tag{3}$$

a representation compatible with the classical beam theory, where (i) $\mathbf{u}$, $\mathbf{v}$ and $\mathbf{w}$ are column-vectors containing the member displacement fields ($u(x,s)$, $v(x,s)$ and $w(x,s)$), (ii) $(\cdot)_{,x} \equiv \partial(\cdot)/\partial x$, (iii) $\mathbf{U}$, $\mathbf{V}$ and $\mathbf{W}$ are matrices containing the cross-section displacement profiles ($u_k(s)$, $v_k(s)$ and $w_k(s)$) in each row, and (iv) $\boldsymbol{\phi}$ is a column-vector whose components are modal amplitude functions ($\phi_k(x)$), defined along the member length ($0 \le x \le L$).

The GBT equilibrium equations, written in the matrix form, are given by

$$\mathbf{C}\boldsymbol{\phi}_{,xxxx} - \mathbf{D}\boldsymbol{\phi}_{,xx} + \mathbf{B}\boldsymbol{\phi} - \lambda W_m^o \mathbf{X}_m \boldsymbol{\phi}_{,xx} = \mathbf{0} \tag{4}$$

where W_m^o are generalised pre-buckling stress resultants (known *a priori*), λ (load parameter) is the problem eigenvalue and the matrices appearing in system (4) read

$$\mathbf{C} = E\int_0^b [t\,\mathbf{U}^{\mathrm{T}}\mathbf{U} + \tfrac{t^3}{12}\mathbf{W}^{\mathrm{T}}\mathbf{W}]\,ds$$

$$\mathbf{D} = G\int_0^b [\tfrac{t^3}{3}(\mathbf{W}_{,\mathrm{s}}^{\mathrm{T}}\mathbf{W}_{,\mathrm{s}}) - \tfrac{\nu}{2(1-\nu)}(\mathbf{W}_{,\mathrm{ss}}^{\mathrm{T}}\mathbf{W} + \mathbf{W}^{\mathrm{T}}\mathbf{W}_{,\mathrm{ss}})]\,ds$$

$$\mathbf{B} = \tfrac{E}{12(1-\nu^2)}\int_0^b t^3\,\mathbf{W}_{,\mathrm{ss}}^{\mathrm{T}}\mathbf{W}_{,\mathrm{ss}}\,ds \qquad \mathbf{X}_m = \int_0^b \tfrac{Et}{\mathbf{C}_m}(\mathbf{V}^{\mathrm{T}}\mathbf{U}_m^o\mathbf{V} + \mathbf{W}^{\mathrm{T}}\mathbf{U}_m^o\mathbf{W})ds \tag{5}$$

Once the displacement field components (**U**, **V** and **W**) are known, it is possible to calculate the matrices **C**, **D**, **B** and **X** appearing in system (4), which constitutes a straightforward (but time/effort consuming) task. Moreover, it should be mentioned that all the above four matrices are *fully populated*, which means that system (4) is *highly* coupled, a fact that considerably complicates its solution and, more important than that, the interpretation of the results obtained. Indeed, the physical meaning of the various matrix components is far from obvious, even in the case of rather trivial and well-known phenomena (*e.g.*, bending). In order to take full advantage of all the GBT potential, mostly concerning the clarity and physical interpretation of the results, the above matrices must be rendered "as simple as possible", a goal achieved through the simultaneous diagonalisation of matrices **C** and **B**.

3.2 Determination of the Local-Plate and Distortional Modes

Consider the eigenvalue problem

$$(\mathbf{B} - \lambda_k\mathbf{C})\,\mathbf{y}_k = \mathbf{0} \tag{6}$$

which has $n+m+1$ eigenvalues λ_k – the first *four* are *null*. The following remarks are appropriate:

(i) $\lambda_k=0$ ($k=1,...,4$) correspond to the vector space defined by *4* eigenvectors $\dot{\mathbf{y}}_k$ associated with cross-section *rigid-body* motions – axial extension, major and minor axis bending and torsion.

(ii) $\lambda_k>0$ ($k=5,...,n+1$) correspond to $n-3$ eigenvectors $\dot{\mathbf{y}}_k$ associated with cross-section in-plane *deformation*, characterised by warping and fold-line motions – *distortional modes*.

(iii) $\lambda_k>0$ ($k=n+2,...,n+m+1$) correspond to m eigenvectors $\dot{\mathbf{y}}_k$ associated with cross-section in-plane *deformation* without warping and fold-line motions – *local-plate modes*.

For illustration purposes, consider the cross-section discretisation shown in Figure 3, which leads to the identification of *13* (conventional) deformation modes – Figures 6(a)-(b) show the in-plane deformed configurations and warping displacement profiles of *2* (≡*n-3*) *distortional* modes. Figure 7, on the other hand, displays the in-plane deformed configurations of the *7 local-plate* modes (*7*≡*m*) – note that they involve no fold-line motions (natural node displacements).

Figure 6. Lipped Channel Distortional Modes: (a) In-Plane Configurations and (b) Warping Profiles

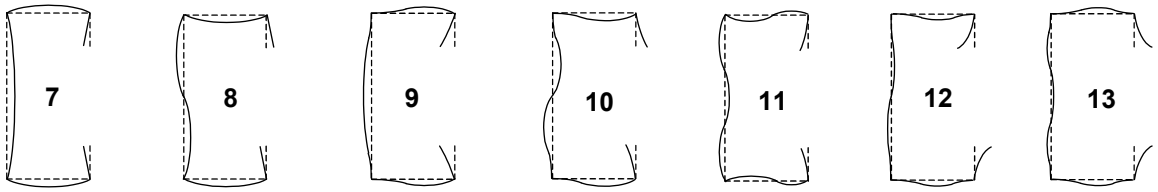

Figure 7. Lipped Channel Local-Plate Modes: In-Plane Deformed Configurations

Because one has $\lambda_k=0$ ($k=1,...,4$), any vector obtained through a linear combination of $\dot{\mathbf{y}}_1$, $\dot{\mathbf{y}}_2$, $\dot{\mathbf{y}}_3$ and $\dot{\mathbf{y}}_4$ is also an eigenvector of system (6). To obtain the *four rigid-body* deformation modes, one considers the sub-matrix $\dot{\mathbf{Y}}_I$ (formed by the first four eigenvectors of (6)) and the transformed matrices $\dot{\mathbf{C}}$ and $\dot{\mathbf{D}}$, defined by

$$\dot{\mathbf{Y}}_I = [\dot{\mathbf{y}}_1 \quad \dot{\mathbf{y}}_2 \quad \dot{\mathbf{y}}_3 \quad \dot{\mathbf{y}}_4] \qquad \dot{\mathbf{C}} = \dot{\mathbf{Y}}_I^T \, \mathbf{C} \, \dot{\mathbf{Y}}_I \qquad \dot{\mathbf{D}} = \dot{\mathbf{Y}}_I^T \, \mathbf{D} \, \dot{\mathbf{Y}}_I \tag{7}$$

3.3 Determination of the Torsion Mode

Consider the eigenvalue problem ($\dot{\mathbf{C}}$ and $\dot{\mathbf{D}}$ are the transformed matrices in (7))

$$(\dot{\mathbf{D}} - \lambda_k \dot{\mathbf{C}})\, \mathbf{y}_k = \mathbf{0} \tag{8}$$

which has *4* eigenvalues λ_k – the first *three* are *null*:

$\lambda_k=0$ ($k=1,...,3$) correspond to a vector space defined by *3* eigenvectors $\dot{\mathbf{y}}_k$ associated with cross-section *rigid-body* motions having *no twisting* rotation – extension, major/minor axis bending.

(ii) $\lambda_4>0$ corresponds to *one* eigenvector $\dot{\mathbf{y}}_4$ associated with a cross-section *rigid-body* motion *with twisting* rotation – *torsion mode*. Figure 8 shows the in-plane deformed configuration and warping displacement profile of this mode.

(a) (b)

Figure 8. Lipped Channel Torsion Mode: (a) In-Plane Configuration and (b) Warping Profile

Then, one determines matrix (of dimension $(n+m+1)\times 4$)

$$\ddot{\mathbf{Y}} = \dot{\mathbf{Y}}_{\mathbf{I}}\,\mathbf{Y} = \dot{\mathbf{Y}}_{\mathbf{I}}\,[\mathbf{y}_1 \quad \mathbf{y}_2 \quad \mathbf{y}_3 \quad \mathbf{y}_4] = [\ddot{\mathbf{y}}_1 \quad \ddot{\mathbf{y}}_2 \quad \ddot{\mathbf{y}}_3 \quad \ddot{\mathbf{y}}_4] \tag{9}$$

which stems from the product between $\dot{\mathbf{Y}}_{\mathbf{I}}$ (expression (7)) and $\mathbf{Y}$ (the 4×4 transformation matrix formed by the eigenvectors of system (8)). The fact mentioned in item (i) above implies that any vector given by a linear combination of $\ddot{\mathbf{y}}_1$, $\ddot{\mathbf{y}}_2$ and $\ddot{\mathbf{y}}_3$ is also an eigenvector of system (6) and, thus, the sub-system corresponding to the first three rows and columns remains fully populated. In order to characterise the last three rigid-body modes, one must consider the sub-matrix $\ddot{\mathbf{Y}}_{\mathbf{II}}$ (formed by the first three columns of $\ddot{\mathbf{Y}}$) and the transformed matrices $\ddot{\mathbf{C}}$ and $\ddot{X}$ (of dimension 3×3), given by

$$\ddot{\mathbf{Y}}_{\mathbf{II}} = [\ddot{\mathbf{y}}_1 \quad \ddot{\mathbf{y}}_2 \quad \ddot{\mathbf{y}}_3] \qquad \ddot{\mathbf{C}} = \ddot{\mathbf{Y}}_{\mathbf{II}}^{\mathrm{T}}\,\mathbf{C}\,\ddot{\mathbf{Y}}_{\mathbf{II}} \qquad \ddot{\mathbf{X}} = \ddot{\mathbf{Y}}_{\mathbf{II}}^{\mathrm{T}}\,\mathbf{X}\,\ddot{\mathbf{Y}}_{\mathbf{II}} \tag{10}$$

3.4 Determination of the Bending and Axial Extension Modes

Consider now the eigenvalue problem ($\ddot{\mathbf{C}}$ and $\ddot{\mathbf{X}}$ are the transformed matrices in (10))

$$(\ddot{\mathbf{X}} - \lambda_k \ddot{\mathbf{C}})\,\mathbf{y}_k = \mathbf{0} \tag{11}$$

which has *3* eigenvalues λ_k – the *first* is *null*:

$\lambda_k=0$ ($k=1$) corresponds to *one* eigenvector $\dot{\mathbf{y}}_1$ associated with a cross-section *rigid-body* motion with *no* in-plane cross-section *displacements – axial extension mode*.

(ii) $\lambda_2>\lambda_3>0$ correspond to *two* eigenvectors $\mathbf{y}_2$ and $\mathbf{y}_3$ associated with cross-section *rigid-body* motions *with* in-plane cross-section *displacements – major and minor axis bending modes*.

Figure 9 shows the lipped channel section in-plane deformed configurations and warping displacement profiles of the axial extension and major/minor axis bending modes. Finally, one must determine the matrix (of dimension $(n+m+1)\times3$)

$$\ddot{\mathbf{Y}} = \ddot{\mathbf{Y}}_{\mathbf{II}}\,\mathbf{Y} = \ddot{\mathbf{Y}}_{\mathbf{II}}\,[\mathbf{y}_1 \quad \mathbf{y}_2 \quad \mathbf{y}_3] = [\ddot{\mathbf{y}}_1 \quad \ddot{\mathbf{y}}_2 \quad \ddot{\mathbf{y}}_3] \tag{12}$$

which stems from the product between $\ddot{\mathbf{Y}}_{\mathbf{II}}$ (expression (10)) and $\mathbf{Y}$ (3×3 transformation matrix formed by the eigenvectors of system (11)).

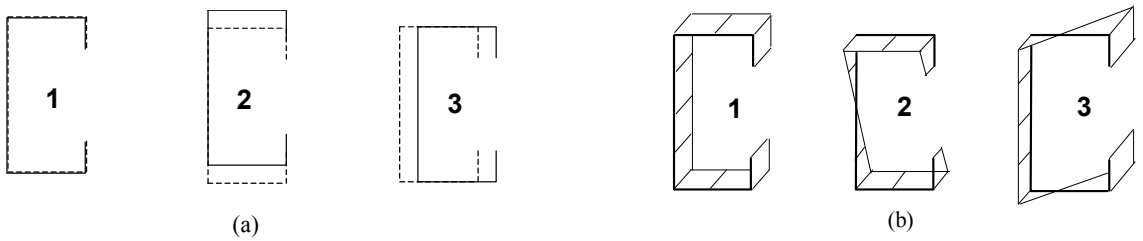

Figure 9. Lipped Channel Extension and Bending Modes: (a) In-Plane Configurations and (b) Warping Profiles

3.5 Modal Form of GBT Equations

Finally, assembling matrices $\ddot{\mathbf{Y}}$, $\ddot{\mathbf{Y}}$ and $\dot{\mathbf{Y}}$ into a $(n+m+1)\times(n+m+1)$ global transformation matrix leads to

$$\widetilde{\mathbf{Y}} = \left[\mathbf{Y}_{III} \quad \mathbf{Y}_{II} \quad \mathbf{Y}_{I}\right] = \left[\ddot{\mathbf{y}}_{1} \quad \ddot{\mathbf{y}}_{2} \quad \ddot{\mathbf{y}}_{3} \quad \ddot{\mathbf{y}}_{4} \quad \dot{\mathbf{y}}_{5} \quad \cdots \quad \dot{\mathbf{y}}_{n+m+1}\right] \tag{13}$$

where each column $\widetilde{\mathbf{y}}_k$ corresponds to one of the $n+m+1$ orthogonal *deformation modes*. In the particular case of the lipped channel section shown in Figure 3, the mixed vector $\mathbf{y}$ (*i.e.*, involving warping $\widetilde{u}_i$ and flexural $\widetilde{w}_j$ displacements) defined by expression (2) has now the modal form

$$\widetilde{\mathbf{y}}_k = \{\widetilde{u}_1 \quad \widetilde{w}_2 \quad \widetilde{u}_3 \quad \widetilde{w}_4 \quad \widetilde{u}_5 \quad \widetilde{w}_6 \quad \widetilde{w}_7 \quad \widetilde{w}_8 \quad \widetilde{u}_9 \quad \widetilde{w}_{10} \quad \widetilde{u}_{11} \quad \widetilde{w}_{12} \quad \widetilde{u}_{13}\}^{\mathsf{T}} \tag{14}$$

The components of $\widetilde{\mathbf{y}}_k$ are (i) the warping displacements at the natural nodes ($\widetilde{u}_i$, *i=2, 3, 5, 9, 11* and *12*) and (ii) the flexural displacements at the intermediate nodes ($\widetilde{w}_j$, *j=4, 6, 7, 8* and *10*) and lip end nodes ($\widetilde{w}_j$, *j=1* and *13*), which define each deformation mode configuration. Note that local-plate modes (*k=7, ..., 13* – see Figure 7) display null warping displacements and that the corresponding vectors $\widetilde{\mathbf{y}}_k$ are of the form

$$\widetilde{\mathbf{y}}_k = \{\widetilde{w}_1 \;\; 0 \;\; 0 \;\; \widetilde{w}_4 \;\; 0 \;\; \widetilde{w}_6 \;\; \widetilde{w}_7 \;\; \widetilde{w}_8 \;\; 0 \;\; \widetilde{w}_{10} \;\; 0 \;\; 0 \;\; \widetilde{w}_{13}\}^{T} \tag{15}$$

Similarly, the axial extension mode (*k=1* – see Figure 9(a)) exhibits null flexural displacements and the corresponding vector $\widetilde{\mathbf{y}}_1$ is given by ($\widetilde{u}_i = 1$)

$$\widetilde{\mathbf{y}}_1 = \{0 \;\; \widetilde{u}_2 \;\; \widetilde{u}_3 \;\; 0 \;\; \widetilde{u}_5 \;\; 0 \;\; 0 \;\; 0 \;\; \widetilde{u}_9 \;\; 0 \;\; \widetilde{u}_{11} \;\; \widetilde{u}_{12} \;\; 0\}^{\mathsf{T}} \tag{16}$$

All the remaining modes (*i.e.*, bending, torsion and distortional modes – see Figures 6, 8 and 9) are characterised by non-null warping and flexural displacements – the corresponding vectors display the general form given in (14). After completing this task, one obtains the set of $n+m+1$ ("mixed" u-w) eigenvectors, each associated with a specific cross-section *deformation mode*. Then, all four (fully populated) matrices $\mathbf{C}$, $\mathbf{D}$, $\mathbf{B}$ and $\mathbf{X}$ must be transformed by means of the operations

$$\widetilde{\mathbf{C}} = \widetilde{\mathbf{Y}}^{\mathsf{T}}\,\mathbf{C}\,\widetilde{\mathbf{Y}} \qquad \widetilde{\mathbf{D}} = \widetilde{\mathbf{Y}}^{\mathsf{T}}\,\mathbf{D}\,\widetilde{\mathbf{Y}} \qquad \widetilde{\mathbf{B}} = \widetilde{\mathbf{Y}}^{\mathsf{T}}\,\mathbf{B}\,\widetilde{\mathbf{Y}} \qquad \widetilde{\mathbf{X}} = \widetilde{\mathbf{Y}}^{\mathsf{T}}\,\mathbf{X}\,\widetilde{\mathbf{Y}} \tag{17}$$

The components of the transformed matrices $\widetilde{\mathbf{C}}$, $\widetilde{\mathbf{D}}$, $\widetilde{\mathbf{B}}$ and $\widetilde{\mathbf{X}}$ are the *cross-section modal mechanical properties*, namely (i) the axial, bending, torsional and warping stiffness values (global modes) and (ii) several less familiar properties with no obvious mechanical meaning (distortional and local-plate modes). The GBT system (4) then acquires the modal form

$$\widetilde{\mathbf{C}}\widetilde{\boldsymbol{\phi}}_{,xxxx} - \widetilde{\mathbf{D}}\widetilde{\boldsymbol{\phi}}_{,xx} + \widetilde{\mathbf{B}}\widetilde{\boldsymbol{\phi}} - \lambda\widetilde{W}_m^o\widetilde{\mathbf{X}}_m\widetilde{\boldsymbol{\phi}}_{,xx} = \mathbf{0} \tag{18}$$

As for the nature of the matrices appearing in Eq. 18, it is worth noting that:

(i) $\widetilde{\mathbf{C}}$, $\widetilde{\mathbf{D}}$, $\widetilde{\mathbf{B}}$ are stiffness matrices concerning generalised warping, torsion and transverse bending (cross-section in-plane deformation), respectively – see the expressions in (5).

(ii) $\widetilde{\mathbf{X}}_m$ (*m=1*, *2*, *3*, *4*) are geometric stiffness matrices that account for the influence of the interaction between the longitudinal normal stresses associated with the pre-buckling deformation mode *m* (stress resultant $\widetilde{W}_m^o$) and the in-plane cross-section strains. Moreover, it is also worth noting that the generalised stress resultants $\widetilde{W}_m^o$ (deemed uniform along the member length) can be either (ii_1) axial compressive forces ($\widetilde{W}_1^o = N$), (ii_2) major/minor axis bending moments ($\widetilde{W}_2^o = M_I$ or $\widetilde{W}_3^o = M_{II}$), ($ii_3$) bi-moments ($\widetilde{W}_4^o = B$) or ($ii_4$) any combination of the above. The diagonalisation procedure described earlier is only capable of *reducing* the strong coupling of the GBT differential equilibrium equation system (18). However, the non-diagonal symmetric geometric stiffness matrix $\widetilde{\mathbf{X}}_m$ always causes mode coupling effects in buckling analyses.

The solution of the eigenvalue problem defined by system (18) is either (i) a closed-form analytical expression satisfying the homogeneous differential equations and associated boundary conditions (*exact* solution, only possible in a few cases) or (ii) yielded by applying a numerical discretisation method, which replaces the member buckling mode by a linear combination of pre-defined shape functions (*approximate* solution, always possible). In the first case, *exact* solutions may only be obtained for simply supported members (end sections locally/globally pinned and free to warp). In such case (the one dealt with in this work), the buckling modes vary longitudinally accordingly to sinusoidal functions of the type

$$\widetilde{\phi}_k = d_k sin\left(\frac{n_s \pi x}{L}\right) \tag{19}$$

where n_s is the half-wave number ($n_s=1$ in this work) and L is the member length. The participation of deformation mode k in a cross-section deformed configuration associated with a given buckling mode depends on the ratio between the corresponding $\widetilde{\phi}_k$ value and the sum of all such values – obviously, this ratio varies along the member length. Therefore, it seems plausible to quantify the contribution of mode k to the member buckling mode by means of a *participation factor* given by

$$p_k = \frac{\int_0^L \left|\widetilde{\phi}_k\right|}{\sum_{i=1}^{n}\left(\int_0^L \left|\widetilde{\phi}_i\right|\right)} \tag{20}$$

which correspond to the ratio between the *averages* of $\widetilde{\phi}_k$ and of the sum of all modal amplitudes. The GBT-based modal participation diagrams presented in this work are based on this definition. Note that in simply supported members, an alternative participation factor definition involving only the mid-span modal amplitudes can also be used – it yields p_k values that are very similar to the ones obtained with the ratio defined in (20).

4. OVERVIEW OF cFSM

4.1 FSM Essentials

The semi-analytical Finite Strip Method (FSM) was developed to analyse prismatic plated structures (*e.g.*, [11]). The most important features of FSM are (i) discretisation into *strips* (long and narrow rectangular plates), (ii) selection of longitudinal shape functions that constitute (exact or approximate) solutions of the problem, obviously satisfying its boundary conditions, and (iii) the use of polynomial transverse shape functions, as is typically done in FEM (Finite Element Method) applications. These features are responsible for the fact that the FSM (i) involves a significantly smaller number of d.o.f. than the FEM (*i.e.*, requires less input data and computational effort) and (ii) can only be effectively applied to certain types of regular structures (due to the need to pre-define adequate longitudinal shape functions).

Since the advantages of the FSM can be fully exploited when performing buckling analyses of thin-walled members, while its restrictions pose no significant problems (in most cases), this method became popular in the last decades. In buckling applications, the stiffness of each strip stems from a combination of (i) small deflection plate bending (d.o.f. w) and (ii) membrane plane stress (d.o.f. u and v). As for the shape functions adopted, they are (i) standard cubic polynomials for the transverse flexural d.o.f., (ii) linear polynomials for the transverse membrane d.o.f. and (iii) sinusoidal functions in the longitudinal direction. In an individual strip, the plate bending and membrane behaviours are completely uncoupled, even though the assembly of the strips into the member global stiffness matrix causes coupling between the membrane (in-plane) and flexural (out-of-plane) behaviours. Moreover, the choice of longitudinal functions implies that the member end sections are locally/globally pinned and may warp freely – thus, one only obtains solutions for thin- walled member buckling problems exhibiting these classical end support conditions. Note, however, that the FSM is capable of handling more complex end support conditions (not addressed in this work). Finally, note that there at least two FSM codes widely available to the technical/scientific community, namely THIN-WALL [12] and CUFSM [13] – moreover, it is worth mentioning that the cFSM presented and discussed in this work is implemented and available in the latest version of CUFSM [14].

To obtain the buckling modes of a thin-walled member by means of the FSM, one must solve a generalised eigenvalue problem that can be written as

$$\mathbf{K_e \Phi} = \mathbf{\Lambda K_g \Phi} \tag{21}$$

where (i) $\mathbf{K_e}$ and $\mathbf{K_g}$ are the global elastic and geometric stiffness matrices, (ii) $\mathbf{\Phi} = [\boldsymbol{\varphi}_1 \quad \boldsymbol{\varphi}_2 \quad \dots \quad \boldsymbol{\varphi}_m]$ is the eigenvector matrix, (iii) $\mathbf{\Lambda} = diag[\lambda_1, \lambda_2, ..., \lambda_m]$ is the eigenvalue matrix and (iv) $m=4\times n$ is the number of d.o.f. – note that the exact evaluation of $\mathbf{K_e}$ and $\mathbf{K_g}$ is reported in [15].

4.2 Mode Definition

The separation between *global* (G), *distortional* (D), *local* (L) and *other* (O) deformation modes can be carried out through the application of the following three mechanical criteria (Table 4 shows which criteria must be satisfied by the different deformation modes. In the context of the cFSM, "deformation mode" may sometimes mean "deformation mode family" or "deformation mode space" – this was not the case in GBT, where "deformation mode" means a specific cross-section deformed configuration:

(i) Criterion 1. (a) $\gamma_{xy} = 0$, *i.e.*, null membrane shear strains, (b) $\varepsilon_x = 0$, *i.e.*, null transverse extensions, and (c) the axial displacements v are linear along each wall mid-line (i.e., between two main nodes).
(ii) Criterion 2. (a) $v \neq 0$, i.e., the warping displacement are not null along the whole cross-section, mid-line, and (b) the cross-section is in transverse flexural equilibrium.
(iii) Criterion 3. $\kappa_{xx} = 0$, i.e., there is no transverse flexure.

Table 4. Mode definition in cFSM: criteria that must be satisfied by the different deformation modes.

	G modes	**D** modes	**L** modes	**O** modes
Criterion 1 – Vlasov's hypothesis	Yes	Yes	Yes	No
Criterion 2 – Longitudinal warping	Yes	Yes	No	–
Criterion 3– Undistorted section	Yes	No	–	–

4.3 Concept of Constraint Matrices for Modal Decomposition

Implementation of the criteria given in Table 4 is completed through the application constraint matrices for each of the modes that "force" the FSM general displacement field (expressed in terms of *m* d.o.f.) to satisfy the relevant criteria, thus leading to "reduced d.o.f." displacement fields. In order to achieve this goal, one establishes relationships between the nodal displacements of the form

$$\mathbf{d} = \mathbf{R_M d_M} \tag{22}$$

where (i) $\mathbf{d}$ is a general *m*-element displacement vector, (ii) $\mathbf{d_M}$ is a displacement vector in the reduced space, and (iii) $\mathbf{R_M}$ is the constraint matrix associated with a certain deformation mode and responsible for enforcing deformations in accordance with a set of pre-defined mechanical assumptions (criteria) – note that subscript "M" identifies the deformation mode or modes and may stand for G, D, L, O or GD, GDL, etc. It should be noted that, since the $\mathbf{d_M}$ vector belongs to a "reduced d.o.f." space, it is not necessarily directly associated with the original nodal displacements – instead, $\mathbf{d_M}$ should be viewed simply as a vector in generalised coordinates.

In general, there is an infinite number of vectors satisfying Eq. 22 for a given $\mathbf{R_M}$ constraint matrix, which means that all of them lay in the same vector (or function, to be more precise) *space* – a *sub-space* of the original FSM d.o.f. space. Any such sub-space can be conveniently defined by means of a set of linearly independent *base vectors* – note that the column vectors of $\mathbf{R_M}$ can also be viewed as base vectors. Hence, the vector space defined by the base vectors associated with a given mode (included in the relevant $\mathbf{R_M}$) will also be designated as G, D, L or O space – one may also speak about a GD space (the reunion of the G and D spaces), a GDL space (the reunion of the G, D and L spaces), etc. Naturally, the GDLO space coincides with the original FSM d.o.f. space.

Since a buckling mode shape is itself a displacement field (*i.e.*, eigenvectors are displacement vectors), the constraint given by Eq. 22 may also be applied to $\mathbf{\Phi}$. By introducing (22) into (21) and pre-multiplying by $\mathbf{R_M}^T$,

$$\mathbf{R_M}^T\mathbf{K_e R_M \Phi_M} = \mathbf{\Lambda_M R_M}^T\mathbf{K_g R_M \Phi_M} \tag{23}$$

which can be re-written as

$$\mathbf{K_{e,M} \Phi_M} = \mathbf{\Lambda_M K_{g,M} \Phi_M} \tag{24}$$

an equation that is recognisable as a new eigenvalue problem, now posed in the "reduced (constrained) d.o.f." space spanned by the deformation mode or modes under consideration. In the above expression, $\mathbf{K_{e,M}}$ and $\mathbf{K_{g,M}}$ are the linear stiffness and geometric stiffness matrices of the constrained FSM problem.

Since $\mathbf{R_M}$ is an $m \times m_M$ matrix, where m_M is the dimension of the reduced d.o.f. space, $\mathbf{K_{e,M}}$ and $\mathbf{K_{g,M}}$ are $m_M \times m_M$ matrices, much smaller than the $m \times m$ $\mathbf{K_e}$ and $\mathbf{K_g}$. Thus, the application of the constraint can be viewed as a form of model reduction. Finally, $\mathbf{\Lambda_M}$ is an $m_M \times m_M$ diagonal matrix containing the eigenvalues associated only with the mode or modes under consideration, and $\mathbf{\Phi_M}$ is the matrix whose columns are the eigenmodes (or buckling modes).

One defines *pure buckling modes* as the solutions of the constrained eigenvalue problem (24), which (i) are also solutions of the *generalised eigenvalue problem* (21), and (ii) satisfy the constraint Eq. 22. The definition of the various $\mathbf{R_M}$ matrices requires different derivations – while $\mathbf{R_L}$ and $\mathbf{R_O}$ can be defined directly, $\mathbf{R_G}$ and $\mathbf{R_D}$ involve two steps: one first defines $\mathbf{R_{GD}}$, which is then separated into $\mathbf{R_G}$ and $\mathbf{R_D}$.

4.4 Constraint Matrix for GD Modes

As a direct consequence of Criteria 1 and 2, any displacement vector belonging to the GD space can be expressed by its axial displacements – note that the above criteria are *a priori* assumptions of the GBT analyses. In other words, the warping displacements unambiguously define the whole member displacement field. Moreover, since the warping displacements are linear between two main nodes (*i.e.*, within a wall), it suffices to know the axial translations of all main nodes to determine the entire displacement field. Then, (i) it is possible to develop a mathematical relationship between the longitudinal displacement d.o.f. and all the remaining ones, (ii) the number of GD base vectors is equal to the number of main nodes and (iii) any set of n_{main} independent warping displacement profiles may be adopted as a base vector system.

4.5 Separation of G and D Modes

To separate the G and D spaces, it is necessary to perform an additional transformation inside the GD space. Mathematically, one seeks a $\mathbf{H_{GD}} = \left[\mathbf{H_G} \quad \mathbf{H_D}\right]$ transformation matrix that can be used to describe any $\mathbf{d_{GD}}$ in terms of a modal basis formed by a system of base vectors that has the G and D vectors separated, *i.e.*, such that

$$\mathbf{d_{GD}} = \left[\mathbf{H_G} \quad \mathbf{H_D}\right] \begin{bmatrix} \mathbf{d_G} \\ \mathbf{d_D} \end{bmatrix} \tag{25}$$

The column vectors of $\mathbf{H_G}$ and $\mathbf{H_D}$ are, in fact, warping displacement profiles associated with the global and distortional modes. Once $\mathbf{H_G}$ and $\mathbf{H_D}$ are defined, they can be used to calculate the global and distortional buckling modes separately. By considering Eqs 22 and 25, any displacement vector in the *global* or *distortional* space can be expressed as $\mathbf{d=R_G d_G}$ or $\mathbf{d=R_D d_D}$, where $\mathbf{R_G}$ and $\mathbf{R_D}$ are the constraint matrices for the G and D spaces, defined as

$$\mathbf{R_G}=\mathbf{R_{GD}H_G} \qquad \mathbf{R_D}=\mathbf{R_{GD}H_D} \tag{26}$$

4.6 Constraint Matrix for the G Modes

Since the constraint matrix for the global modes is expressed as $\mathbf{R_G=R_{GD}H_G}$ and $\mathbf{R_{GD}}$ is already defined through the satisfaction of Criteria 1 and 2, the only task remaining is to find $\mathbf{H_G}$. Recalling that the

columns of **H** are nodal warping displacements, one must define warping displacement profiles specifically for the G modes. Since, by definition, these modes exhibit no cross-section distortion (see Criterion 3 and keep in mind that the longitudinal displacement profile stems from the pre-defined shape functions), one has *4* global modes, associated with the four cross-section rigid-body motions: (i) longitudinal translation, (ii) two transverse translations and (iii) rotation about the member longitudinal axis passing through the cross-section shear centres – obviously, these deformation modes coincide with the GBT rigid-body ones – their transverse and warping displacement profiles were already shown in Figures 9(a)-(b) and 8(a)-(b).

4.7 Constraint Matrix for the D Modes

Since there is no direct definition currently available for distortional modes, their warping displacement profiles are obtained by imposing that they must be linear independent with respect to the global modes. Independence with the global modes is achieved by satisfying the orthogonality condition

$$\int v_i(x) v_j(x) t(x)\, dx = 0 \tag{27}$$

where the integration is carried over the whole cross-section, $t(x)$ is the wall thickness and $v_i(x)$ and $v_j(x)$ are arbitrary warping functions belonging to the G and D spaces, respectively. Note that the above expression is also employed in the GBT approach, see the first term in matrix **C**, given in (5) (recall that u are warping displacements in the GBT notation). The imposition of the above orthogonality conditions requires some mathematical operations that are not discussed here (see [4, 5]) but lead to the determination of the $\mathbf{H_D}$ matrix, *i.e.*, the warping displacement profiles characterising the distortional modes. Then, the corresponding constraint matrix is given by $\mathbf{R_D}=\mathbf{R_{GD}}\mathbf{H_D}$.

4.8 Constraint Matrix for the L Modes

The constraint matrix $\mathbf{R_L}$ can be defined through the direct application of the criteria defining the L modes, given in Table 4. First, one uses the fact that L modes need not satisfy Criterion 2, which means that (i) all the warping displacements are null and (ii) transverse flexural equilibrium may be violated. At the same time, the enforcement of Criterion 1 leads to a strict relationship between the longitudinal displacements of the main nodes and the transverse displacements of the internal main nodes, which implies that the L modes have no internal main node displacements (only rotations may occur). Then, the consideration of Criterion 1(a) makes it clear that the local u displacements must be null for all strips, *i.e.*, no membrane shear strains can occur in the member. Moreover, only displacements in the local w direction (*i.e.*, normal to the plate strip) are allowed at the nodes that can move (*i.e.*, all but the main nodes 2 to n_{main}-1). Since no other restrictions apply to the L modes, the allowable generalised displacements include (i) local w-direction translations of the external main nodes, (ii) local w-direction translations of the sub-nodes and (iii) rotations of all nodes – all remaining nodal generalised displacements are fully restrained.

A possible and rather convenient way to define the $\mathbf{R_L}$ matrix is to apply FEM-like (or FSM-like) base functions with unit value at appropriate w or θ local d.o.f. and null value at all remaining d.o.f. This procedure is illustrated in Figure 10, for the lipped channel considered throughout this paper (see Figure 3 – *6* main nodes and *5* sub-nodes) – all FEM-like local base functions are shown and one should note that this cFSM discretisation (with *5* sub-nodes) replicates the previous GBT discretisation (with *7* intermediate nodes).

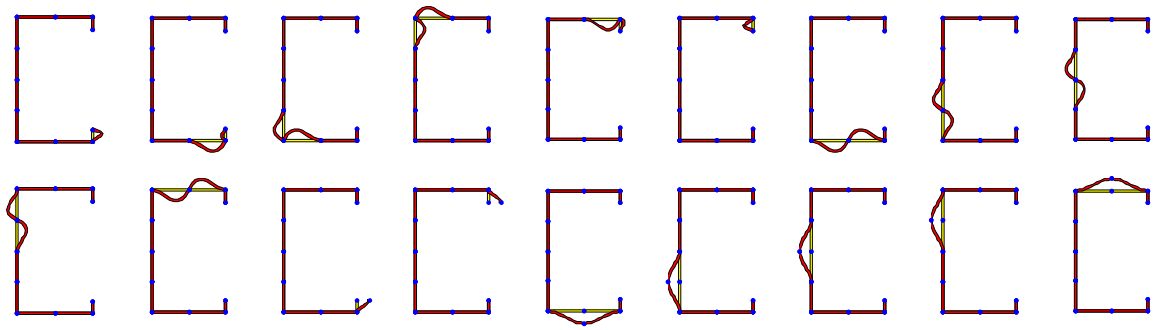

Figure 10. FEM-Like (Natural) Base Functions Considered for the L Modes

4.9 Constraint Matrix for the O Modes

The O-modes are characterised by the fact that they do not satisfy Criterion 1, *i.e.*, (i) the in-plane (membrane) transverse extensions and/or shear strains are not null and (ii) non-linear warping displacement profiles may exist within a wall width (*i.e.*, between adjacent main nodes) – the latter condition is strongly related to the existence of membrane shear strains. The direct application of the above considerations makes it a straightforward task to define a system of independent vectors associated with unit transverse extensions and unit shear strains, as has been done similarly in the GBT approach [16] – since both modes may occur in any strip, the number of the corresponding base vectors must equal $2\times(n-1)$ (twice the number of strips). It is worth mentioning, however, that these types of deformation modes were only considered in the context of GBT-based *post-buckling analysis* (*i.e.*, they were never included in buckling analyses).

It should still be mentioned that this approach, although easy to explain and understand, has a non-negligible drawback: the resulting O space has overlaps with the previously defined sub-spaces (G, D and L spaces). Thus, in order to avoid such overlaps, the O base vectors can be defined in such a way that they must necessarily be orthogonal to the G, D and L ones – the use of modern numerical tools (*e.g.*, definition of null spaces in MATLAB [17]) render the performance of this task quite straightforward.

4.10 Orthogonal Modes

Any pure mode space (G, D, L, etc.) can be defined by means of a multitude of base vector systems. However, it is certainly convenient to define special base vector systems, among which orthogonal systems have considerable practical importance. A convenient way to perform the orthogonalisation is to solve the constrained eigenvalue problem defined by Eq. 24, assuming that the applied stresses are uniformly distributed along the cross-section mid-line. The columns of the resulting $\boldsymbol{\Phi}_{\mathbf{M}}$ matrix contain the unit member pure buckling modes, which are obviously orthogonal to each other and span the sub-space under consideration – thus, any $\mathbf{d}_{\mathbf{M}}$ vector belonging to the reduced d.o.f. space can be expressed as a linear combination of them,

$$\mathbf{d}_{\mathbf{M}} = \boldsymbol{\Phi}_{\mathbf{M}}\mathbf{c}_{\mathbf{M}} \tag{28}$$

where (i) $\boldsymbol{\Phi}_{\mathbf{M}}$ is the $m_M \times m_M$ matrix of the orthogonal modes and (ii) the $\mathbf{c}_{\mathbf{M}}$ vector components define the contributions of the various modes (*i.e.*, $\mathbf{c}_{\mathbf{M}}$ is the *modal coordinate vector*). It is worth noting that the $\boldsymbol{\Phi}_{\mathbf{M}}$ matrix can also be interpreted as a transformation matrix that, when applied to $\mathbf{R}_{\mathbf{M}}$, effectively transforms the solution of the constrained eigenvalue problem into the unit-member axial mode base system, but expressed in the original nodal d.o.f. space – indeed, the incorporation of (28) into (22) leads to

$$\mathbf{d} = \mathbf{R_M d_M} = \mathbf{R_M \Phi_M c_M} = \mathbf{C_M c_M} \tag{29}$$

which demonstrates that any nodal displacement vector $\mathbf{d}$ lying in a given M sub-space can be expressed as a linear combination of the $\mathbf{C_M}$ matrix column vectors – this matrix, which should not be confused with the GBT $\mathbf{C}$ matrix, is just a transformed form of the corresponding restraint matrix $\mathbf{R}$ whose columns are orthogonal and expressed in the original FSM nodal displacement space.

Once the orthogonal modes are defined both in the reduced and original d.o.f. spaces, any pure mode space can still be further reduced by eliminating one or more of those modes (*i.e.*, columns of the $\mathbf{\Phi_M}$ or $\mathbf{C_M}$ matrices) – if only one mode is kept, this procedure ultimately leads to *individual buckling modes*.

It should be noted that, in general, the $\mathbf{R_M}$ matrices (and, therefore, also their orthogonal versions $\mathbf{\Phi_M}$ or $\mathbf{C_M}$) depend on the member length. However, it is possible to introduce length-independent orthogonal modes, by carrying out the above orthogonalisation procedure for a unit-length member, where "unit-length" is defined so that one has $k_r=r\pi/a=1$, which leads to a real length equal to $a=r\pi$, where r is the number of sinusoidal half-waves considered. The advantage of a length-independent orthogonal base system is that it is unique for a specific cross-section and, thus, directly comparable with the GBT modes. Figures 11 and 12 show the G, D and first nine L orthogonal modes, for a unit-length member with the illustrative lipped channel section.

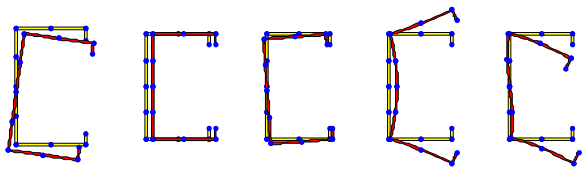

Figure 11. Global and Distortional Length-Independent Orthogonal Modes
(In-Plane Deformed Shapes)

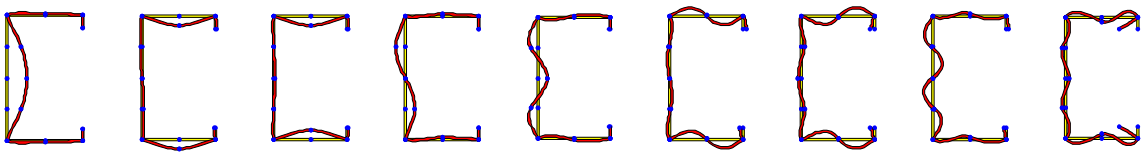

Figure 12. First Nine Local Length-Independent Orthogonal Modes
(In-Plane Deformed Shapes)

4.11 Mode Contribution Calculation

The most important use of the orthogonal (deformation) modes is the calculation of modal contributions to a general unconstrained member buckling mode (or even to any other member deformed configuration). The formulae required to perform this task, in the context of the entire GDLO space, can be obtained directly from Eq. 29 (one just needs to replace subscript M with GDLO). However, since the $\mathbf{C_{GDLO}}$ matrix columns are eigenvectors that can be arbitrarily scaled, the calculation of the modal contributions (participations) requires the definition of a suitable *normalisation*.

Various normalisation procedures are possible (*e.g.*, see [18]), the one adopted here is called *work normalisation*, since it is based on the work done by a unit force on the deformed (orthogonal) shape. To achieve this, one incorporates an orthogonal mode $\boldsymbol{\varphi}$ into the eigenvalue problem defined by Eq. 21 and pre-multiplies both sides by $\boldsymbol{\varphi}^{\mathbf{T}}$, thus leading to

$$\frac{1}{\lambda}\boldsymbol{\varphi}^{T}\mathbf{K}_{e}\boldsymbol{\varphi} = \boldsymbol{\varphi}^{T}\mathbf{K}_{g}\boldsymbol{\varphi} \tag{30}$$

where the right hand side is the work done by the unit compressive force (if $\mathbf{K_g}$ is calculated for a unit stress evenly distributed along the cross-section mid-line), which becomes unitary through the appropriate scaling of the $\boldsymbol{\varphi}$ vector. Then, if one uses the normalised orthogonal mode vectors to construct the linear combination defined in Eq. 29, the elements of vector $\mathbf{c_{GDLO}}$ provide the contributions of the deformation modes to the member buckling mode – the corresponding *relative contribution* of a particular mode can be obtained by means of the expression

$$\left|c_i\right| \Big/ \sum_{all} \left|c_i\right| \tag{31}$$

where c_i denotes the component of the $\mathbf{c_{GDLO}}$ vector under consideration. Similarly, the joint contribution of a family of deformation modes (*i.e.*, global, distortional or local modes) is defined as

$$\sum_{mode} \left|c_i\right| \Big/ \sum_{all} \left|c_i\right| \tag{32}$$

Concerning the orthogonality, it is worth noting that it is always satisfied within a given mode family, as a direct consequence of their derivation. However, modes belonging to different families are not necessarily orthogonal to each other – this fact accounts for a small degree of arbitrariness in the calculation of the modal contributions (participations). However, since experience shows that the modes calculated according to the above-described procedure are nearly orthogonal, the calculation of the modal participating factors is certainly applicable in practice – note that the GBT deformation modes also are not fully orthogonal displacement fields.

5. ILLUSTRATIVE NUMERICAL RESULTS

5.1 General Comparison

In order to enable a better grasp of the concepts and procedures presented before, GBT and cFSM are next employed to investigate the *single-wave* buckling behaviour of thin-walled lipped channel columns and beams having (i) cross-section dimensions b_{web}*=100 mm*, b_{flange}*=60 mm*, b_{lip}*=10 mm*, t*=2 mm*, (ii) pinned (locally and globally) and free to warp end sections, and (iii) the (steel) elastic constants E*=210 GPa* and ν*=0.3*. The results obtained are presented in (i) Figures 13 and 14 (*columns*) and (ii) Figures 15 and 16 (*beams* under major axis bending) and will be discussed next.

The curves depicted in Figures 13 and 15 provide the variation of the buckling load ($\lambda_b P \equiv P_b$) or buckling moment ($\lambda_b M_Z \equiv M_b$) with the member length L (represented in logarithmic scale), obtained by means of analyses that include (i) only individual deformation modes or combinations of a few of them (top curves and corresponding dots) or (ii) all the deformation modes simultaneously (bottom thick solid curves and black dots) – the curves and dots provide GBT and cFSM results, respectively. Concerning the top curves and dots, one has (i) dotted curves and thick white dots for the local-plate buckling results, (ii) dashed-dotted curves and grey dots for the distortional buckling results and (iii) thin solid curves and thin white dots for the global buckling results. As for Figures 14 (columns) and 16 (beams), they make it possible to visualise the "degree of participation" of each individual mode (GBT) or each mode family (cFSM) in the member buckling mode.

After observing Figures 13 and 14, dealing with the *column* buckling behaviour, one concludes that:

(i) As usual, local-plate buckling dominates for short columns ($L<18$ *cm*), distortional buckling prevails for intermediate-length columns ($18<L<75$ *cm*) and flexural-torsional or flexural buckling modes occur for the longer columns ($L>250$ *cm*). In the length range $75<L<250$ *cm*, the columns buckle in distortional-flexural-torsional mixed modes.

(ii) There is a virtually perfect agreement between the results yielded by the GBT (thick solid curve) and cFSM (black dots) that take into account all deformation modes simultaneously. As far as the local-plate and distortional minima are concerned, the differences between the buckling load values provided by the two approaches are *0.25%* and *0.80%* respectively. Concerning global buckling, the differences are of the same order of magnitude (*e.g.*, *0.78%* for $L=226$ *cm*).

(iii) Despite the fact that the GBT modal participation diagram provides more detailed information concerning the contribution of each deformation mode to the column buckling mode (actually, the cFSM diagram shows the relative contributions of the deformation mode families L, D, G and O), the two diagrams are quite similar. The minor discrepancies detected in Figure 14 can be attributed to the different definitions of the GBT and cFSM participation factors.

Finally, the results presented in Figures 15 and 16, concerning the *beam* buckling behaviour, show that:

(i) Now, local-plate buckling only dominates for very short beams ($L<10$ *cm*), while lateral-torsional buckling prevails for the long ones ($L>250$ *cm*). As for the beams with small-to-intermediate lengths ($10<L<90$*cm*), they buckle in distortional modes. Lastly, the buckling modes of the not-too-long beams ($90<L<250$ *cm*) are mixed distortional-flexural-torsional – however, the distortional contribution tends to be smaller than in the columns.

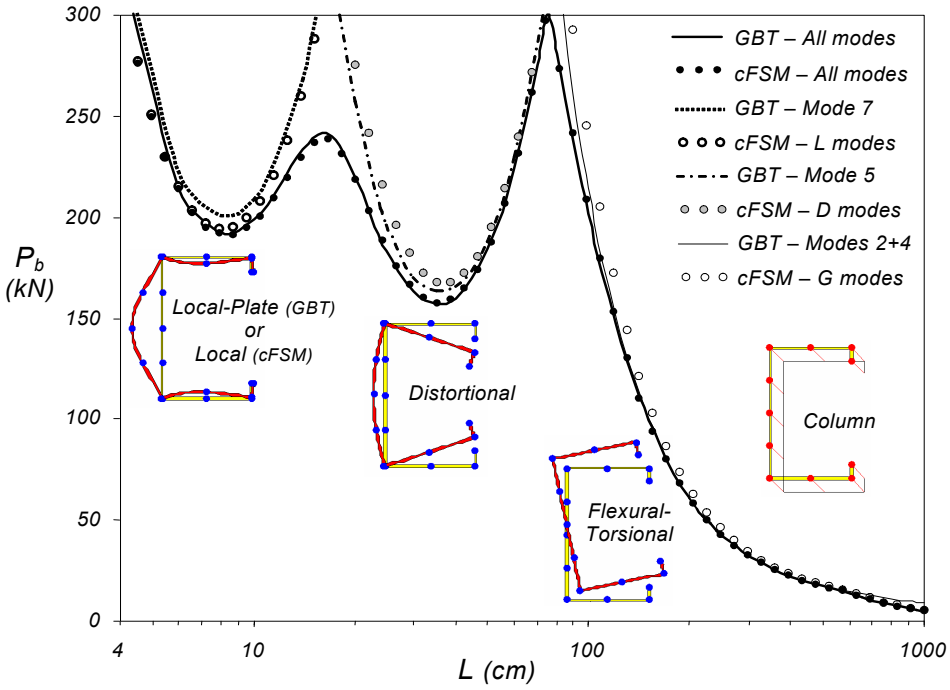

Figure 13. Variation of the Buckling Load P_b with the Column Length L

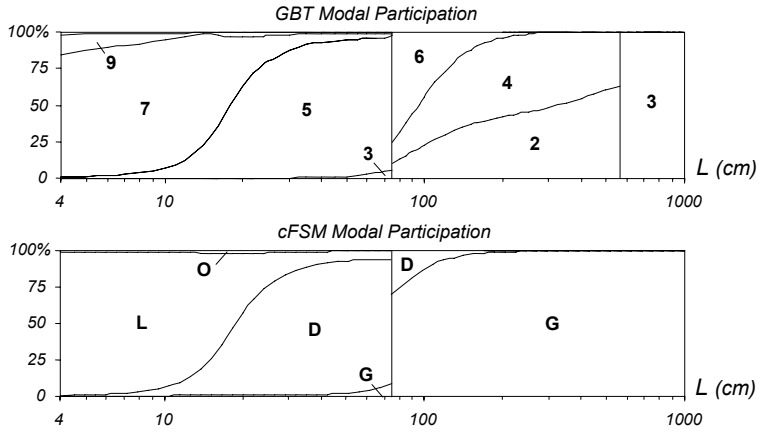

Figure 14. Column GBT and cFSM Modal Participation Diagrams

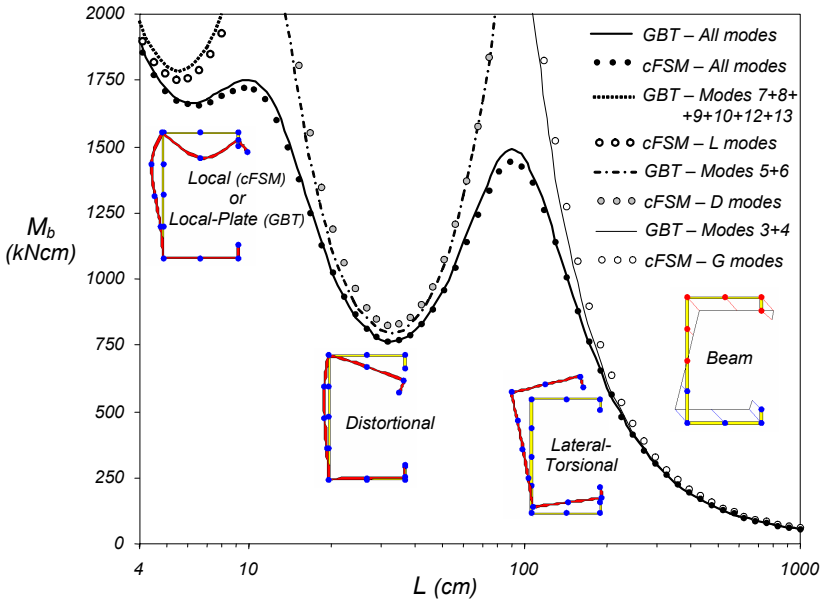

Figure 15. Variation of the Buckling Moment M_b with the Beam Length L

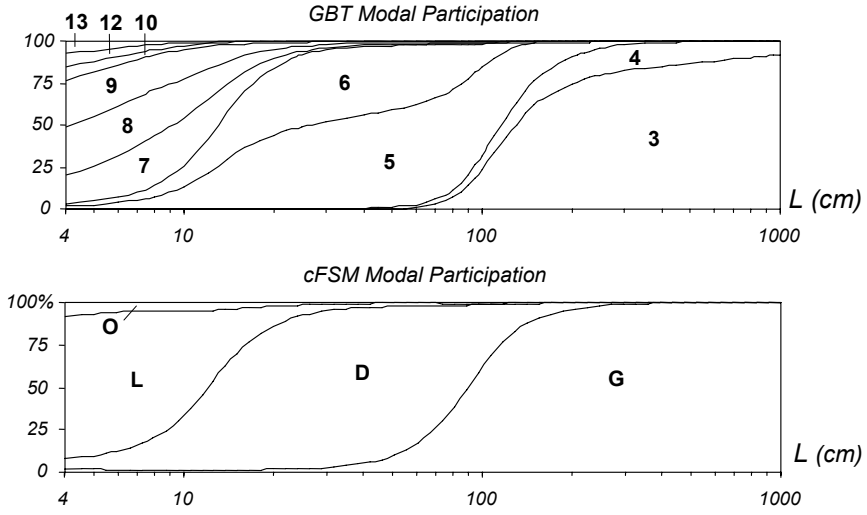

Figure 16. Beam GBT and cFSM Modal Participation Diagrams

(ii) The results provided by the GBT and cFSM all-mode analyses (thick solid curve and black dots) are again very close. In particular, it is worth mentioning that the buckling moment differences are equal to *1.35%* and *0.25%* for the local-plate and distortional minima, respectively, and similarly small for the beams buckling in lateral-torsional modes (*e.g.*, *0.56%* for *L=298.4 cm*).

(iii) Once more, the GBT and cFSM modal participation diagrams are rather similar. Note that the cFSM L-mode, D-mode and G-mode domains practically coincide with the reunions of the GBT sub-domains associated with deformation modes **7**+**8**+**9**+**10**+**12**+**13**, **5**+**6** and **3**+**4**, respectively. Only the cFSM O-mode domain has no GBT counterpart, due to the fact that no shear or transverse extension modes were included in the GBT analyses – this may explain the small differences between the two sets of M_b values (the cFSM ones are slightly lower).

5.2 The Role of Kinematic and Constitutive Modelling

During the course of this comparative study between the GBT and cFSM analyses of the buckling behaviour of unbranched open thin-walled members, it was found that some of the small discrepancies detected in the numerical results yielded by the two approaches can be traced back to basic mechanical assumptions embedded in them. Indeed, while cFSM logically views the member as an assembly of interconnected plates (the FSM is based on folded-plate theory), GBT tries to accommodate, as much as possible, the classical beam model format – these different perspectives have two main consequences:

(i) Concerning the kinematic (strain-displacement) relation dealing with the longitudinal extensions, cFSM takes into account the non-linear terms associated with all the displacements. On the other hand, GBT does not incorporate the non-linear term stemming from the longitudinal displacements (the same as the classical beam models) – however, note that this term is only non-negligible for members with very small lengths, of very little (if any) practical interest.

(ii) Concerning the plane stress constitutive (stress-strain) relationship, cFSM adopts the exact one, which implies that the longitudinal normal stresses and extensions are related by $E/(1-\nu^2)$. On the other hand, GBT employs an approximate 2D constitutive relation that replaces the above elastic constant by the Young's modulus E, in order to replicate the 1D stress state characterising the classical beam theories – in the case of steel (ν=0.3), this corresponds to a 9% increase that is directly reflected in the member stiffness values associated with applied longitudinal normal stresses. This stiffness increase can also be conveniently interpreted as an "artificial" increase of the corresponding cross-section geometric properties, namely the area A, the major/minor moments of inertia I and the warping constant C_w.

In the case of the global flexural buckling of thin-walled columns, the first author [19] showed that the above mechanical assumption differences are responsible for buckling load drops that (i) increase as the column length decreases and (ii) are only non-negligible for very short columns – nevertheless, the cFSM critical stresses tend to $E/(1-\nu^2)$ as the column length approaches zero, a value that is in sharp contrast with the infinite one yielded by GBT (and also by the Euler formula).

In view of what was mentioned in the previous paragraphs, it becomes clear that the effect of the membrane axial stiffness change (*i.e.*, E vs. $E/(1-\nu^2)$) on the member buckling stress depends on how relevant is the role played by the applied longitudinal normal stresses – thus, it seems logical to anticipate the following, concerning the relation between the GBT and cFSM pure-mode (G, D and L) buckling stresses:

(i) The larger differences correspond to column global flexural (F) buckling, since only longitudinal normal stresses are involved.

(ii) In column torsional (T) or flexural-torsional (FT) buckling and in beam lateral-torsional (LT) buckling, the relevant stresses are longitudinal normal (flexure and warping torsion) and shear (Saint-Venant torsion) – the relative importance of the shear stresses obviously grows with the participation of torsion in the column/beam buckling mode. This means that the differences must be smaller than in the F buckling case (*9%*), particularly so in T buckling.

(iii) Since distortional (D) buckling involves cross-section distortion and wall bending, relevant shear and transverse normal stresses are present, together with the longitudinal normal ones. Therefore, the differences will again be smaller than *9%*.

(iv) Since local (L) buckling is associated exclusively with wall (transverse) bending, only transverse normal stresses are involved. Thus, the differences between cFSM and GBT buckling stresses are bound to be rather small.

In order to assess the correctness of the above predictions, one presents next numerical results concerning simply supported lipped channel steel ($E=210$ *MPa* and $\nu=0.3$) columns and beams with (i) cross-section dimensions $b_{web}=150$ *mm*, $b_{flange}=60$ *mm*, $b_{lip}=15$ *mm*, $t=2$ *mm* and (ii) lengths comprised between *10* and *10000 mm*. The curves and dots depicted in Figures 17 to 19 provide the GBT and cFSM buckling stresses corresponding to the G, D and L buckling of columns (first two modes) and beams (first mode only) – note that this is only possible due to the unique modal nature of the two approaches. The observation of these numerical results prompts the following remarks (note that the length is represented in logarithmic scale):

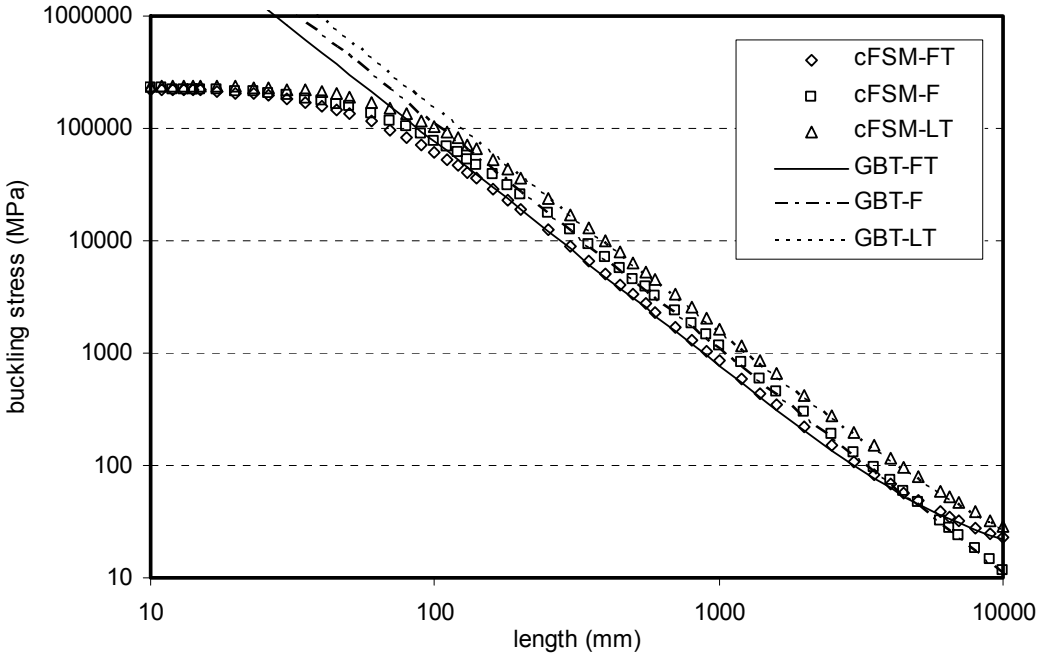

Figure 17. Buckling Stresses Associated with Column and Beam Global Buckling

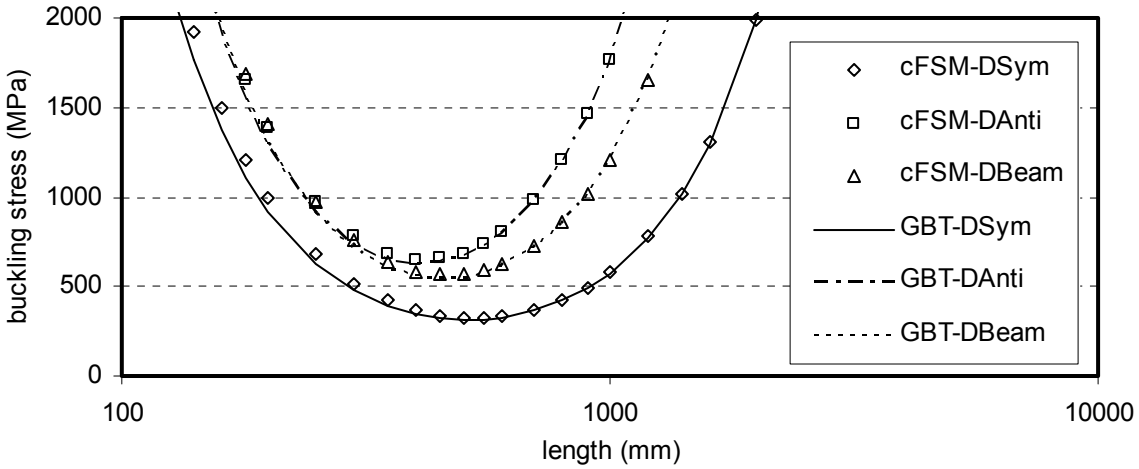

Figure 18. Buckling Stresses Associated with Column and Beam Distortional Buckling

(i) As expected, the cFSM global buckling stresses converge to $E/(1-\nu^2)$ as the column/beam length approaches zero. Naturally, the differences are only non-negligible for small lengths – *e.g.*, for F buckling one has *1%* and *3%* differences for column lengths of *700 mm* and *400 mm*. (Since global buckling very rarely, if ever, governs in this small length range, this fact has little practical relevance.)

(ii) There is another expected discrepancy between the GBT and cFSM global buckling stresses, which is hardly visible in Figure 17 but can be clearly observed in Figure 20, which shows the percentage differences between the two sets of values (calculated with respect to the cFSM ones): the cFSM values are always higher than their GBT counterparts for long columns/beams – since global buckling controls for this length range, these differences have some practical relevance. Moreover, one notices that the differences (ii_1) remain practically constant, at *9%*, for the column F buckling and (ii_2) decrease with the length for column FT and beam LT buckling (*4%* and *6%*, for a *10 m* length) – this is due to the growing relevance of the shear stresses (in comparison with the longitudinal normal ones).

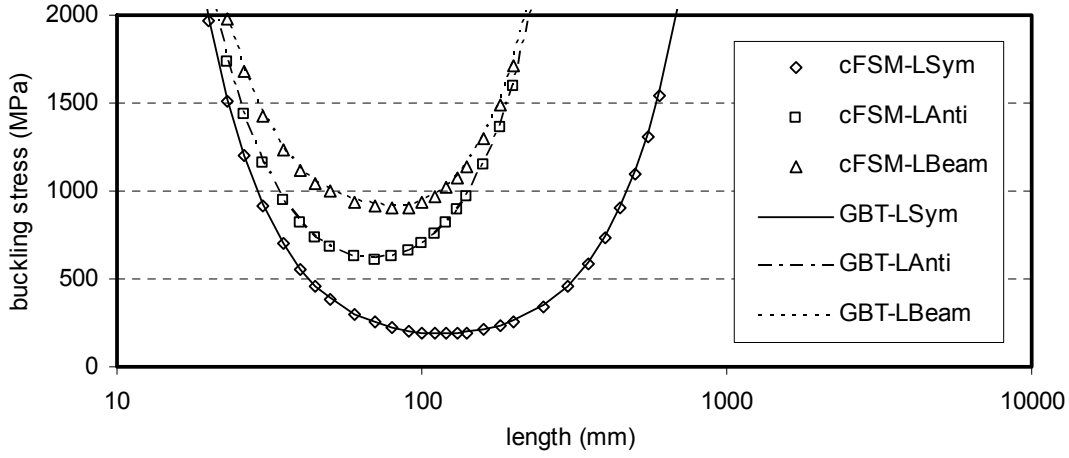

Figure 19. Buckling Stresses Associated with Column and Beam Local Buckling

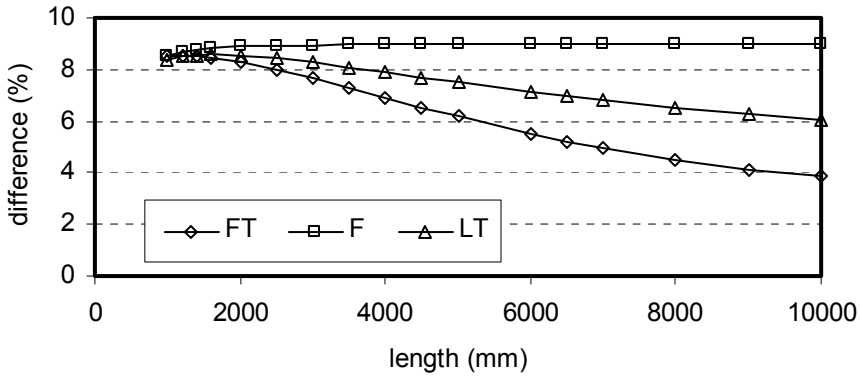

Figure 20. Percentage Difference Between the GBT and cFSM Global Buckling Stresses

(iii) The buckling stress curves displayed in Figure 18 concern the column symmetric (first) and anti-symmetric (second) distortional modes, as well as the beam only distortional mode. As correctly anticipated, the cFSM buckling stresses are always higher than the GBT ones. The percentage differences (again calculated with respect to the cFSM values) are shown in Figure 21 and one observes that they decrease with the column/beam length – a fairly abrupt drop (*8%* to *1%*) in the *150-800 mm* length range, followed by a much smoother one (*1%* to about *0%*) up to a length close to *1600 mm*.

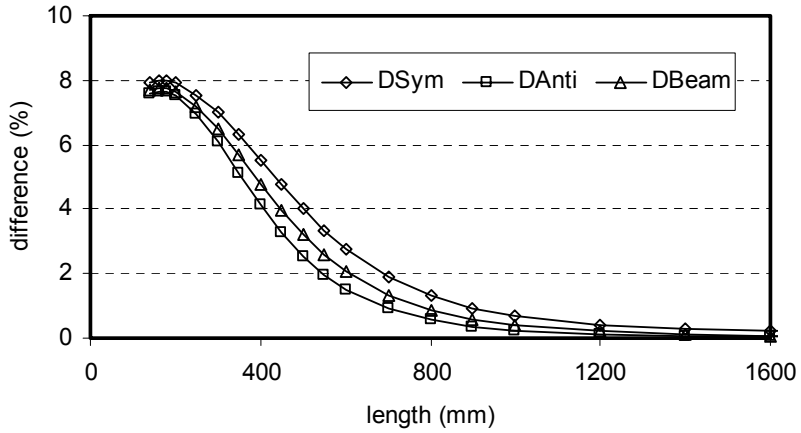

Figure 21. Percentage Difference Between the GBT and cFSM Distortional Buckling Stresses

(iv) As in the distortional case, the buckling stress curves displayed in Figure 19 concern the column symmetric and anti-symmetric (first and second) local modes, together with the beam only one. Once more as predicted, the differences between the cFSM and GBT buckling stresses are very small, regardless of the column/beam length – they never exceed *1%* and would probably be even lower if one considered more refined discretisations (*i.e.*, more sub/intermediate nodes). Note that the interpretation of intermediate nodes (GBT) and sub-nodes (cFSM), as well as the associated base functions, are slightly different – this implies that GBT and cFSM discretisations involving the same number of intermediate/sub nodes do not provide exactly the same approximation. Since, in theory, the GBT and cFSM buckling stresses should be identical (the differences would stem only from numerical reasons), it is a bit surprising to observe that the GBT values are consistently higher than the cFSM ones. This is most likely due to the fact that the GBT local-plate deformation modes are not as "purely local" as the cFSM ones (the GBT orthogonalisation procedure slight spoils their "purity" [1]) – this may be viewed as "additional constraints" that lead to a (minute) increase in the member wall transverse bending stiffness.

6. CONCLUSION

It is well known that unbranched open thin-walled members are generally prone to three types of instability: global, distortional and local (or local-plate) buckling. The proper identification of a given (pure or mixed) buckling mode nature is crucial, since the member post-buckling behaviour, imperfection-sensitivity and ultimate strength strongly depend on it – moreover, the design methods to estimate the member load-carrying capacity also rely heavily on its buckling behaviour nature. Currently, there are two approaches to analyse the buckling behaviour of unbranched open thin-walled members that are able to formally decompose and identify the different buckling phenomena: Generalised Beam Theory (GBT) and the constrained Finite Strip Method (cFSM).

GBT originated as an extension of classical beam theory that was enhanced to include (i) additional warping displacement fields consistent with distortional buckling (first) and (ii) transverse bending displacement fields consistent with local-plate buckling (later). On the other hand, the cFSM has its roots in the semi-analytical FSM, whose plate strips were subsequently constrained to "force" the buckling mode nature – it is based the same mechanical assumptions adopted by GBT (to enhance its displacement fields), which are treated as constraints applied to the FSM general displacement fields. While the GBT formulation does not depend on the longitudinal displacement fields, which makes it applicable to members exhibiting a variety of end support conditions, the cFSM is a specialisation of the semi-analytical FSM method (and not of a general purpose finite element) and, therefore, only provides solutions for simply supported members.

The GBT solution is embodied in a generalised version of the member differential equation system (see (4)) and the simultaneous diagonalisation of two of its matrices (**C** and **B**) constitutes a key step in the GBT derivation – it makes it possible to transform the solution from a nodal space to a *modal* one (see (18)). A very important consequence of these formulation and transformation is the generalisation of the cross-section geometrical properties beyond A (area), I (second moment of area) and C_w (warping constant) to cover distortional and local-plate buckling – this is a unique GBT feature. After performing the above simultaneous matrix diagonalisation, the ensuing **C**, **D** and **B** matrices describe the cross-section mechanical behaviour (linear elastic stiffness), while the geometric stiffness matrix **X** depends on the applied stresses.

The cFSM follows from a typical FSM stability solution (see (21)), where the linear elastic stiffness ($\mathbf{K_e}$) and geometric ($\mathbf{K_g}$) stiffness matrices are formulated on the basis of plate strips containing in-plane membrane (plane stress) and classical Kirchhoff plate bending behaviours. The associated general deformation fields may be constrained, as shown in Eqs. 23 and 24, thus providing a decomposition of the general solution space into G, D, L, and O sub-spaces. A full transformation to a modal basis, analogous to the GBT one, can be applied through the consideration of orthogonal modes for a member of unit length – this procedure was described in subsection 4.10 but not employed to obtain the numerical results presented in this work.

Both GBT and the cFSM provide means to assess the contributions (or participation factors) of the various deformation modes in the member buckling mode shapes – while GBT uses the average of the modal amplitudes along the member length, various options are possible within the cFSM – among them, the one similar to GBT quantifies the contribution of a given mode family as the ratio between the work done by a unit axial force on that mode family and the total work of the same unit force associated with the member buckling mode under consideration. The illustrative numerical results presented and discussed in the paper showed that both GBT and the cFSM are able to decompose the buckling modes and identify the associated modal contributions – as far as the buckling analysis of simply supported thin-walled members, GBT and cFSM offer essentially the same capabilities. Although the numerical results yielded by the two approaches were shown to correlate very well, the small

differences detected prompted a further investigation aimed at understanding their origin. It was found that the (fairly minute) discrepancies stem from the different modelling of (i) the kinematic (strain-displacement) relation dealing with the longitudinal extensions and (ii) the plane stress constitutive (stress-strain) relationship – the most relevant effect is the change in membrane axial stiffness from E (GBT) to $E/(1-\nu^2)$ (cFSM). Moreover, it was possible to predict, and validate numerically, how these modelling differences influence the various member buckling stresses – the effect (i) is most prominent in column flexural buckling (buckling stress differences of *9%* in steel members), (ii) is also felt (but to a lesser extent) in column flexural-torsional, beam lateral-torsional and column/beam distortional buckling, and (iii) practically does not exist in column/beam local buckling.

ACKNOWLEDGEMENTS

The research work reported in this paper was conducted under the financial support of the TéT Port-5/2005 Hungarian-Portuguese Intergovernmental Science and Technology Cooperation Program, the OTKA K62970 project of the Hungarian Scientific Research Fund and the János Bolyai Research Scholarship of the Hungarian Academy of Sciences – this financial support is gratefully acknowledged.

REFERENCES

[1] Schardt, R., "Verallgemeinerte Technische Biegetheorie", Springer Verlag, Berlin, 1989, (German).

[2] Camotim, D., Silvestre, N., Gonçalves, R. and Dinis, P.B., "GBT Analysis of Thin-Walled Members: New Formulations and Applications", Thin-Walled Structures: Recent Advances and Future Trends in Thin-Walled Structures Technology, J. Loughlan (Ed.), Canopus Publishing, Bath, 2004, pp. 137-168.

[3] Camotim, D., Silvestre, N., Gonçalves, R. and Dinis, P.B., "GBT-based Structural Analysis of Thin-walled Members: Overview, Recent Progress and Future Developments", Advances in Engineering Structures, Mechanics and Construction (SMCD 2006 – Waterloo, 14-17/6), Pandey, M., Xie, W.-C., Chu, L. (Eds.), Springer, pp. 187-204, 2006.

[4] Ádány, S. and Schafer, B.W., "Buckling Mode Decomposition of Single-Branched Open Cross-Section Members via Finite Strip Method: Derivation", Thin-Walled Structures, 2006, Vol. 44, No. 5, pp. 563-584.

[5] Ádány, S. and Schafer, B.W., "Buckling Mode Decomposition of Single-Branched Open Cross-Section Members via Finite Strip Method: Application and Examples, Thin-Walled Structures, 2006, Vol. 44, No. 5, pp. 585-600.

[6] Ádány, S. and Schafer, B.W., "A Full Modal Decomposition of Thin-Walled, Single-Branched Open Cross-Section Members via the Constrained Finite Strip Method, Journal of Constructional Steel Research, 64 (1), pp. 12-29, 2008. (doi:10.1016/j.jcsr.2007.04.004).

[7] Ádány, S., Silvestre, N., Schafer, B.W. and Camotim, D., "Buckling Analysis of Unbranched Thin-Walled Members: Generalised Beam Theory and Constrained Finite Strip Method", Book of Abstracts of III European Conference on Computational Mechanics: Solids, Structures and Coupled Problems in Engineering (III ECCM – Lisboa, 5-9/6), C.A.M. Soares, et al. (Eds.), Springer, Lisboa, 2006, Vol. 679 (Full Paper in CD-ROM Proceedings).

[8] Ádány, S., Silvestre, N., Schafer, B.W. and Camotim, D., "Buckling Analysis of Unbranched Thin-Walled Members Using cFSM and GBT: A Comparative Study", Proceedings of International Colloquium on Stability and Ductility of Steel Structures (SDSS 2006 – Lisboa, 6-8/9), Camotim, D. Silvestre, N. Dinis, P.B. (Eds.), IST Press, 2006, pp. 205-212.

[9] Ádány, S., Silvestre, N., Schafer, B.W. and Camotim, D., "On the Identification and Characterisation of Local, Distortional and Global Buckling Modes in Thin-Walled Members Using the cFSM and GBT Approaches", Proceedings of the 6th International Conference on Steel & Aluminium Structures (ICSAS'07 – Oxford, 24-27/7), Beale, R. (Ed.), 2007. pp. 760-767.

[10] Silvestre, N., "Generalised Beam Theory: New Formulations, Numerical Implementation and Applications, Ph.D. Thesis, IST-Technical University of Lisbon, 2005. (Portuguese)

[11] Cheung, Y.K. and Tham, L.G., The Finite Strip Method, CRC Press, Boca Raton, 1998.

[12] Papangelis, J.P. and Hancock, G.J, Cross-Section Analysis and Finite Strip Analysis and Direct Strength Design of Thin-Walled Structures – THIN-WALL (version 2.1), Center for Advanced Structural Analysis, School of Civil and Mining Engineering, University of Sydney, 2005. (Its website is http://www.civil.usyd.edu.au/case/thinwall)

[13] Schafer, B.W., "Elastic Buckling Analysis of Thin-Walled Members (FSM) – CUFSM (Version 2.6), Johns Hopkins University, 2003. (Freely Available at the Website http://www.ce.jhu.edu/bschafer/)

[14] Schafer, B.W., "Elastic Buckling Analysis of Thin-Walled Members (cFSM) – CUFSM (Version 3.12), Johns Hopkins University, 2006. (Freely Available at the Website http://www.ce.jhu.edu/bschafer/)

[15] Schafer, B.W. and Ádány, S., "Buckling Analysis of Cold-Formed Steel Members Using CUFSM: Conventional and Constrained Finite Strip Methods", Proceedings of 18th International Specialty Conference on Cold-Formed Steel Structures (Orlando, 26-28/10), 2006, LaBoube, R., Yu, W.W. (Eds.), pp. 39-54.

[16] Silvestre, N. and Camotim, D., "Non-Linear Generalised Beam Theory for Cold-Formed Steel Members", International Journal of Structural Stability and Dynamics, 2003, Vol. 3, No. 4, pp. 461-490.

[17] Mathworks Inc., MATLAB Users Guide (Version 7), Natick, USA, 2005, (http:/www.mathworks.com)

[18] Ádány, S., Silvestre N., Schafer, B.W. and Camotim, D., "Buckling Mode Identification of Thin-Walled Members: A Comparison Between cFSM and GBT Approaches", Fifth International Conference on Coupled Instabilities in Metal Structures (CIMS 2008 – Sydney, 23-25/6), 2008, pp. 249-256

[19] Ádány, S., "Flexural Buckling of Thin-Walled Columns: Discussion on the Definition and Calculation", Proceedings of International Colloquium on Stability and Ductility of Steel Structures (SDSS 2006 – Lisboa, 6-8/9), Camotim, D., Silvestre, N., Dinis, P.B. (Eds.), IST Press, pp. 249-258, 2006.